

Article

Transition from tunneling leakage current to molecular tunneling in single-molecule junctions

Junyang Liu,¹ Xiaotao Zhao,² Jueting Zheng,¹ Xiaoyan Huang,¹ Yongxiang Tang,¹ Fei Wang,¹ Ruihao Li,¹ Jiuchan Pi,¹ Cancan Huang,^{3,4} Lin Wang,^{3,5} Yang Yang,^{1,***} Jia Shi,¹ Bing-Wei Mao,¹ Zhong-Qun Tian,¹ Martin R. Bryce,^{2,**} Wenjing Hong,^{1,6*}

¹State Key Laboratory of Physical Chemistry of Solid Surfaces, College of Chemistry and Chemical Engineering, iChEM, Pen-Tung Sah Institute of Micro-Nano Science and Technology, Xiamen University, Xiamen 361005, China.

²Department of Chemistry, Durham University, Durham DH1 3LE, United Kingdom.

³Department of Chemistry and Biochemistry, University of Bern, Bern 3012, Switzerland.

⁴Present address: Department of Mechanical and Process Engineering, ETH Zurich, Zurich 8006, Switzerland.

⁵Present address: School of Materials Science and Technology, China University of Geosciences, Beijing 100083, China.

⁶Lead Contact

*Correspondence: whong@xmu.edu.cn

**Correspondence: m.r.bryce@durham.ac.uk

***Correspondence: yangyang@xmu.edu.cn

SUMMARY

The tunneling leakage current will be a major quantum obstacle during miniaturization in the semiconductor industry down to the scale of several nanometers. At this scale, to promote charge transport and overcome the tunneling leakage current between the source and drain terminals, molecular electronic junctions offer opportunities by inserting molecules between these two electrodes. Employing a series of oligo(aryleneethynylene) (OAE) molecules, here we investigate the transition from tunneling leakage current to molecular tunneling in the single-molecule devices using mechanically controllable break junction (MCBJ) technique, and the transition distances of the OAE molecular junctions were determined and even down to 0.66 nm for OAE2 molecular junction, which demonstrates that the intrinsic charge transport properties of a single-molecule device can be outstripped from the tunneling leakage current. Consequently, molecular electronic devices show the potential to push the ultimate limit of miniaturization to the scale of several angstroms.

Keywords: molecular electronics, break junction, tunneling leakage, molecular tunneling, single-molecule conductance

INTRODUCTION

Semiconductor industry is committed to scaling down the silicon-based state-of-art CMOS (complementary metal-oxide-semiconductor) transistors to sub-5 nm nodes in the near future.¹⁻³ Moore's Law, however, has not been the only priority in semiconductor industry because of some inevitable quantum obstacles which hinder the further miniaturization and integration, such as the tunneling leakage current and the thermal dissipation.^{4,5} Meanwhile, various "More-than-Moore" and "Beyond CMOS" strategies have been considered. Among them, molecular electronics provides an alternative opportunity to use molecules as primary elements for building single-molecule electronic components in electronic circuitry,⁶⁻¹² where the molecule possess the intrinsic charge transport properties to overcome the tunneling leakage between the same scale of nanogap distance. Hence, molecular electronics offers a chance to fabricate two-terminal functional molecular devices for new designs of key switching elements in electronic circuits,¹³⁻¹⁶ such as the functions of signal processing and data storage. Nevertheless, during the shrinking of the nanogap between two-terminal devices, tunneling leakage current are dominated by the through-space tunneling between the source and drain terminals, which increases exponentially with the terminal distance and become non-negligible, as described in Figure 1A.^{17,18} Therefore, the

determination of transition distance between the intrinsic molecular tunneling and the tunneling leakage current through single-molecule devices is of fundamental significance, and will enhance the understanding of the technical limitations and boundaries for using single-molecule components as electronic devices.

To explore the critical transition distance, molecular ruler which represents a family of molecules with a different number of repeating units, offers the chance to investigate charge transport through single-molecule devices at varying distances between the source and drain terminals. By employing molecule ruler, previous studies had revealed that the mechanism of charge transport through single-molecule devices evolved from tunneling to hopping,¹⁹⁻²¹ which can be considered as the upper size limit of tunneling based molecular electronics. Additionally, recent studies exploring conformational effects in single-molecule junctions demonstrated that there is also a significant dependence of conductance on distance, because the molecular conformations vary as the nanogap size changes.²²⁻²⁵ Thus the entire junction configurations are mechanically controlled using break junction techniques, which offers further fine tuning in charge transport through the extended molecular rulers. With the ability to accurately tune nanogap distance between the two-terminal devices, break junction techniques facilitate the extraction of intrinsic molecular tunneling properties from tunneling leakage current.

In this paper, we investigate the dominant size ranges of through-space tunneling and molecular tunneling through single-molecule junctions (Figure 1A) using mechanically controllable break junction (MCBJ) technique (Figure 1B).²⁶⁻³⁰ A family of oligo(aryleneethynylene) (OAE) derivatives with a different number of repeating units (Figure 1C)²¹ are used as molecular rulers to investigate the transition from through-space tunneling to molecular tunneling. The OAEs with repeating units of phenylethynyl are highly conjugated, rigid molecular systems which have been widely studied as benchmark molecular wires for single-molecule electronics.^{27,30,31} For longer OAEs such as OAE₄ and OAE₅, the alkoxy side chains are used to enhance their solubilities in the solvent for single-molecule conductance investigation, which shows no significant variation in the charge transport through OAE backbones.^{21,32,33} The closing process from break junction experiment is extracted to provide the precise determination of the electrode-electrode distance for the conductance-nanogap size correlation. By screening this series of OAE molecules, a correlation of the characterized conductance of the molecules with different lengths and configurations is investigated, and the transition between through-space tunneling and molecular tunneling is quantitatively determined.

RESULTS AND DISCUSSION

Conductance-distance measurement of single-molecule OAE₂ junctions.

Typical conductance-distance curves of the OAE₂ molecule from MCBJ experiments in solution^{24,34,35} are shown in Figure 2A (See Figure 1B and section EXPERIMENTAL PROCEDURES for details). Both opening and closing curves³⁶⁻³⁸ display clear plateaus at around $10^{-3} G_0$ (where G_0 is the conductance quantum which equals $2e^2/h$). A sudden conductance drop to the molecular plateau followed by discrete G_0 steps was observed in the opening process (blue curves in Figure 2A), which suggests the pulling of a gold atomic contact and formation of an initial nanogap from the inevitable snap-back after final rupture of gold-gold atomic chain.^{24,39-41} However, the closing curves exhibit longer plateaus than the opening ones, along with a conductance jump from $10^{-1} G_0$ to tens of G_0 when electrodes approaching back (green curves in Figure 2A). This may suggest a "jump-to-contact" process in the distance scale less than one gold atom,⁴²⁻⁴⁴ where the strong electrical field inside the nanogap induced a rapid joining of the gold terminals.

For quantitative comparison, conductance histograms of both opening and closing processes were established from 2000 continuous cycles without data selection, as shown in Figure 2B. Compared to the histogram from the opening process, the discrete G_0 steps disappear in the closing process, indicating the absence of the formation of a gold atomic chain. In both histograms, the conductance peaks dissipate at around $10^{-4.8} G_0$. Same as our previous work,²⁴ this feature of single-conductance state originated from the configuration with stretched and rigid OAEs backbone and the face-to-face gold electrodes with single-atom atop. While on the other hand, it is noticeable that there is a minor, yet significant, peak shift ($10^{-3.6} G_0$ for opening and $10^{-3.2} G_0$ for closing curves). Moreover, the conductance peak in the closing process also exhibited higher intensity on the higher conductance side. These

findings suggest significantly different evolutions of molecular junctions in the opening/closing process of the two terminals.

To investigate the evolution of molecule tunneling versus distance, the master curves²⁴ of both opening and closing processes were extracted from their corresponding 2D histograms,⁴⁵ as superimposed as black curves on the 2D conductance-distance histograms in Figure 2C and 2D. To describe the statistical behaviour for the conductance-distance trace, master curve helps to find the most probable conductance value for every relative distance. Compared to that of the opening process, there is a more extended molecular conductance cloud in the conductance-distance histogram of the closing process. Besides, a more tilted conductance feature appears at around $10^{-1.5} G_0$, which can be attributed to the contribution of the through-space tunneling.^{17,18} The relative distance distribution determined from the conductance range from $10^{-0.3} G_0$ to $10^{-4.8} G_0$ indicates a 0.5 nm difference in length between the opening curves (peak position at 0.5 nm, inset in Figure 2C) and the closing curves (peak position at 1.0 nm, inset in Figure 2D). This difference suggests the snap-back distance, which is close to previous reports.^{39,40,46} It should be noticed that the distance determined from the closing process is relatively smaller than the length of the **OAE2** molecule.^{23,24} This suggests that at the end of the opening process, the molecular junction will break and snap back into adsorption on a more energetically favorable metal tip.⁶ While at the start of the consequent closing process, the attached molecule will form contact with the opposite electrode to form an extended molecular junction.

Measurement of nanogap size via through-space tunneling.

Because of the inevitable snap-back in opening process, the extraction of the absolute distance between two electrodes remains a challenge. Therefore, the key information to determine molecular configurations will be masked. The closing process, alternatively, provides characterization of the through-space tunneling regime, offers a unique opportunity to determine the absolute distance between the two gold terminals via the through-space tunneling regime. Since there is still a jump-to-contact behaviour of gold atoms which occurs at $10^{-1} G_0$ during the closing process,^{42,43} we fitted the through-space tunneling regime of the master curve in Figure 2D in the range of 10^{-1} to $10^{-3} G_0$. The fitting of the slope provided a tunneling decay constant β_T value of about 10 nm^{-1} (for more details see Supplemental Information 4 and Figure S6). Although from the pure solvent calibration under the same conditions of molecular conductance measurement, we obtained a β_T of about 12 nm^{-1} (compared with a previous result of $\log[\Delta G/G_0]/\Delta z = 5.5 \text{ nm}^{-1}$,³⁴ for more details see Supplemental Information 2 and Figure S2). This difference of β_T originates from the surface energy and barrier height differences between clean gold and molecule assembled gold surfaces.⁴⁷ The intercept was determined to be -0.18 nm when extending the fitting curve, owing to the occurrence of the jump-to-contact process at $10^{-0.78} G_0$ (Supplemental Information 4 and Figure S6). This distance is quite close to the size of a single gold atom, suggesting a rapid joining of the gold terminals in the presence of a strong electrical field in the scale of atomic length.⁴⁸ Since the intercept represents an absolute distance between the two gold terminals, the master curves of the closing process can be calibrated, as shown in the green curve in Figure 2E. Thus, the bottom z-axis is a representation of the absolute distance (size of the nanogap) between the two gold terminals, which is calibrated to a zero original point along with the through-space tunneling fitting labeled by a black dash line (Supplemental Information 4).

Subsequently, the master curve of the opening process (blue curve) was aligned together with that of the closing process (green curve) at the point where molecular junction began to rupture (Figure 2E). Obviously, the master curve of the closing process exhibits two significantly different regimes. The conductance evolution exhibits the through-space tunneling, which is shown with light grey background in Figure 2E, with a slope fitted to be $-4.393 (\log(G/G_0) \text{ nm}^{-1})$. Moreover, the conductance plateau with white background shows the molecular tunneling regime, which evolves a completely different behavior than the through-space tunneling regime according to the electrode distance. Since the adopted molecular system has a relatively rigid delocalized π -conjugated backbone, the conductance will strongly correlate to the adsorption angle θ (see Figure S8 in Supplemental Information) between the conjugated backbone and the electrode surface, resulting from the coupling and interaction between the lateral π -conjugated orbital with the gold electrode.^{23,25,49-51} Quek *et al.* suggested the transmission peak of a 4,4'-bipyridine junction increase with $\cos(\theta)$,²³ and other reports suggest a $\cos^4(\theta)$ correlation.⁴⁹⁻⁵¹ In order to accurately describe the correlation, we use the equation $\log(G/G_0) = \log(A \cdot \cos^4(\theta) + B)$ for the non-linear fitting,

where A , B , n are the constants, and θ can be calculated by $\arcsin(z/d_m)$, for which d_m is the molecular length (see Figure S8 in Supplemental Information). Then, the non-linear fitting to correlate molecular conductance of **OAE2** and the absolute electrode distance can be obtained (see Supplemental Information 4 and Figure S9 for more details). Therefore, for **OAE2**, A , B and n are equal to 2.1×10^{-3} , 3.3288×10^{-4} and 4.3304 , respectively, as plotted in the Figure 2F, where the top z-axis represents the calculated junction angle θ .

These findings suggest that two different tunneling-dominated conductance regimes are present during the closing process. Consequently, the through-space tunneling regime and the non-linear evolution of molecular tunneling regime will cross at the transition distance d_t of 0.66 nm (Supplemental Information 4 and Figure S9). This can be identified as the transition between through-space tunneling and molecular tunneling. As indicated by the black dash line of through-space tunneling in Figure 2F, for **OAE2** junctions, the molecular tunneling conductance prominently outstrips the tunneling leakage current and dominates the charge transport in the range from 0.66 nm to 1.20 nm, demonstrating the potential for future miniaturization and integration using a molecule as the functional unit in an electronic device.

Since the Au-N bond (0.8 nN) is weaker than the Au-Au bond (1.4 nN),⁵² no significant deformation of the electrodes during the stretching process is expected for **OAE2** molecules. Thus, the master curve from the opening process, and the simulated junction evolution from DFT (Density Functional Theory) calculations,²⁴ could be aligned with the closing master curve using the last data point before the rupture of the molecular junction. Both opening and closing curves represent a similar trend to a previous study on the manipulation of atomic gold chains at low temperature,³⁹ which indicated the presence of gold atomic chains at room temperature, benefiting from the mechanical stability of the MCBJ process. Besides, the lengths of the closing curves are longer than the opening ones, suggesting that the closing process may offer some additional opportunity to probe missing configurations masked by the snap-back effect in the opening process. Furthermore, comparing the closing curve with previous DFT simulation work in ref. 24 labeled by orange dots in Figure 2E, the through-space tunneling regime from the closing process agrees with that of the simulation throughout the distance range from 0.18 nm to 0.66 nm. Starting from 0.66 nm until the rupture of the molecular junction, the calculations reveal that the conductance variations on the molecular conductance plateau come from the evolution of molecular configurations as the nanogap is extended.²⁴

The transition from through-space tunneling to molecular tunneling.

Furthermore, by the same process, we explore the transition from through-space tunneling to molecular tunneling for the extended **OAE** series. Figures 3A to 3C show the original 2D conductance-distance histograms of the closing process with their corresponding master curves superimposed for **OAE3**, **OAE4**, **OAE5**, respectively (See Supplemental Information 3 and Figures S3 to S5 for the original 2D histograms and the analyses of opening and closing processes of **OAE3** to **OAE5**). Moreover, the relative displacement distributions of all the **OAE** series extracted from both opening and closing processes are shown in Figure 3D. The distinct difference in plateau length between both processes unambiguously indicates the snap-back effect. Starting from the intercept of the fitting of the through-space tunneling regime, the lengths of the closing processes of molecules **OAE2**, **OAE3**, **OAE4** and **OAE5** are determined to be 1.2 , 1.9 , 2.5 and 3.3 nm, respectively, when adding the calibrated distance (0.18 nm) to their statistical lengths of the closing process in Figure 3D. These data indicate that the most probable closing distances are consistent with the corresponding molecular lengths. Table 1 summarizes the key results of the **OAE** series, along with Figure 3E. It is seen that the length distribution of the closing process falls precisely into the diagonal line to fit the corresponding molecular length.

From all master curves of the closing process of the **OAE** series, the molecular conductance plateau is witnessed at the early stage, then all the curves approach into the through-space tunneling regime with almost the same slope. The abrupt jump-to-contact process, however, does not always exist in all the **OAE** molecules, which might result from the stabilization of the configuration of the gold adatoms by assembling of the surface molecule.⁵³ The same calibration method used for **OAE2** was applied to the other three **OAE** molecules, by adding the intercept and fitting those three master curves, as shown in Supplemental Information 5 and Figure S10. Figure 4A shows the superimposed master curves of the closing processes extracted from 2D conductance-distance histograms of all the **OAE** molecules. Control experiments varying stretching rates and bias voltages demonstrated that the transition still

existed, suggesting the transition is intrinsic in the charge transport through single molecules (for more details see Supplemental Information 6&7 and Figure S12&S13). We chose the **OAE** series extended to **OAE5**, then all the adopted **OAEs** are considered to be dominated by super-exchange tunneling²¹ (for more details see Supplemental Information 8 and Figures S14 and S15). For better comparison, their conductance histograms from closing processes are shown at the right panel of Figure 4A. It is noteworthy that there are small conductance differences comparing them with those from the opening processes. For **OAE2** to **OAE4**, the conductance derived from closing was consistently higher than that from opening. Specifically, for **OAE2** the peak shifts from $10^{-3.6} G_0$ to $10^{-3.2} G_0$, for **OAE3** from $10^{-4.6} G_0$ to $10^{-4.3} G_0$, and for **OAE4** from $10^{-5.8} G_0$ to $10^{-5.3} G_0$ (Supplemental Information Figures S3 to S5). Considering the conductance peaks are composed of all the possible molecular configurations during the opening/closing processes, these differences suggest that, due to the snap-back effect, some configurations are unable to be determined in the break junction experiments where only the opening process was taken into consideration. Especially for **OAE2**, as shown in Figure 2E, the initial stage of molecular tunneling plateau located in the shadowed area, suggested that the molecular configurations with relatively small nanogap²⁴ are missing during the opening process (please see supplemental information 4 and Figure S7 for the junction evolution through the opening and closing processes). In the case of longer molecules, such as **OAE5**, because all the missing configurations behaved as through-space tunneling, no significant peak shift can be observed between the opening and closing histograms and both conductance values are the same ($10^{-7.0} G_0$).

Hence, all the master curves in the through-space tunneling regime are closely overlapped, as labeled by the black dashed line in Figure 4A, suggesting that the adsorption of homologue molecules does not significantly influence the tunneling barrier height. Hence, the overall closing process of all the studied **OAE** molecules can be calculated by summing the total conductance of the through-space tunneling G_t and molecular tunneling G_m , for $\log(G/G_0) = \log((G_t+G_m)/G_0) = \log(10^{-4-393z+A*\cos^9(\arcsin(z/d_m)+B)}$ (Supplemental Information 4&5 and Figures S9 and S10). Therefore, the plotted orange curves for all the closing processes of **OAE** molecules are shown in Figure 4A, which fits their corresponding master curves of the closing processes.

The transition distance d_t from through-space tunneling to molecular tunneling was found to be increased with molecules having larger repeating units. For **OAE3**, **OAE4** and **OAE5**, the distances d_t therein were 0.91 nm, 1.2 nm and 1.5 nm, respectively, as summarized in Figure 4B and Table 1 (for more details see Supplemental Information 5 and Figures S10&S11). This length-dependent transition originates from the competition between the exponentially decreased through-space tunneling and the nonlinearly but more mildly decreased molecular tunneling in these homologous serial molecules. Figure 4B further indicates a guide-line through those 4 dots to act as a boundary where the white area above the line suggests molecular tunneling dominated transport, while the grey area below the line suggests through-space tunneling dominated transport. The transition from through-space tunneling to molecular tunneling is a crucial issue for future single-molecule devices. Within the through-space tunneling dominated regime, the measured properties of the device appeared solely as a tunneling diode, and the contribution from molecular behaviour could hardly be extracted (for more details see Supplemental Information 9 and Figure S16). In addition, the transition distance d_t varies from molecule to molecule, e.g., 0.66 nm for **OAE2** and 1.5 nm for **OAE5**. As summarized in Table 1, we found that the transition distance of **OAE2** is larger than Δz_{open} , while smaller for longer molecules of **OAE3**, **4**, **5**. For short molecule which the snap-back distance is considerable as the molecular length, some configurations of the initial period of molecular tunneling are missing because of the fast snap-back effect of electrodes pair during the opening process, as a consequence, the transition point located in the shadowed area of Figure 2E. While for longer molecules with molecular length are significantly longer than snap-back distance, the snap-back effect would not affect the acquisition of the initial configurations of molecular tunneling during the opening process. When the electrodes pair were further pulled open, the through-space tunneling still outstripped the molecular tunneling conductance that the overall logarithmic conductance evolution show linear behavior in logarithmic scale before the transition.

These findings suggest that in future single-molecule electronics, to use the intrinsic properties of the target molecules, nanogaps within two terminals must reach a certain range of size according to the target molecules to outstrip the tunneling leakage current. The effective nanogap distance range where the single-molecule devices properly function for

each **OAE** molecule is 0.66–1.2 nm for **OAE2**, 0.91–1.9 nm for **OAE3**, 1.2–2.5 nm for **OAE4** and 1.5–3.3 nm for **OAE5**, respectively. The transition distance from molecular tunneling to tunneling leakage varied from the structure of the molecules employed in the junctions (see supplemental information 10 and Figure S17 for another two examples). Indeed, in some extreme cases, the molecular conductance cannot be accurately determined if the conductance of fully-elongated molecular junction is still lower than the tunneling leakage current conductance.^{18,29} Recently, quantum interference effects in single-molecule junctions can significantly change the charge transport properties through minor chemical structural and environmental variations within almost the same molecular length.^{8,29,54,55} The conductance enhancement through constructive quantum interference inside the nanogap offers a potential to significantly surpass the tunneling leakage current and push the limit to an even smaller length scale.⁵⁶

Conclusion

To conclude, the transition distance from molecular tunneling to tunneling leakage current within a series of conjugated **OAE** molecules from 1.2 nm to 3.3 nm has been investigated using MCBJ techniques. We reveal that the through-space tunneling and molecular tunneling dominate the charge transport of a molecular junction within different nanogap sizes, and it can be as small as 0.66 nm before the tunneling leakage current dominates the charge transport for the most conductive **OAE2** molecules. Meanwhile, the charge transport dominated by molecular tunneling also exhibits a different dependence on nanogap size for molecules with different lengths, resulting from the tuning of molecule-electrode interactions by changing the tilt angle of molecular junction.

Furthermore, the semiconductor industry has proposed the tunneling Field Effect Transistor (FET) blueprint for a future sub-2 nm node using quantum-mechanical band-to-band tunneling by ultrathin semiconducting films or nanowires.^{3,57} As the line-width will be very close to the radius of a single germanium atom, which is one of the largest elements adopted in semiconductor industry, it suggests the atomic limit for the miniaturization. While using the “bottom-up” strategy and the tunneling mechanism, molecular electronics offers a probability to bridge the gap of the “top-down” shrinking limit, which demonstrates that the leakage current will dominate until even below 0.66 nm in **OAE2** molecule. These conclusions suggest that conjugated molecules are highly promising materials for future miniaturization of electronic devices.

EXPERIMENTAL PROCEDURES

MCBJ experiments.

For MCBJ experiments, nanogaps were fabricated between a notched, suspended gold wire (0.1 mm diameter, 99.99%, Jiaming, Beijing) fixed onto a spring steel sheet (10 mm×30 mm, thickness 0.25 mm) by a two-component epoxy glue (Stycast 2850 FT with catalyst g). A Kell-F liquid cell assisted by a perfluoroelastomer O-ring was mounted onto the sheet. During the measurements, the sample sheet is bent with a pushing rod, which is driven by a combination of a stepping motor (Zaber NA14B16 linear actuator) and a piezo stack (Thorlab AE0505D18F). The setup is shown in Supplemental Information Figure S1. By applying a DC voltage of 100 mV, the current passing through electrode pairs was measured by a lab-built I-V converter with a sensitivity of ~10 fA. The single-molecule conductance measurements were carried at room temperature in solution containing 0.1 mM of target molecule in a mixture of tetrahydrofuran (THF, Aldrich, p.a.) and 1,3,5-trimethylbenzene (TMB, Aldrich, p.a.), 1:4 (v/v). Further technical details of the MCBJ experiments are given in our previous report.^{24,34}

Data analysis.

Data analyses were conducted by a lab-developed program (WA-BJ code). The program enables the separate analysis of the opening or the closing process for break junction experiments. The construction of 1D histograms and 2D conductance-distance histograms, and the extraction of master curves were thoroughly reported by Hong *et al.*²⁴ The fittings of master curves were conducted by Matlab.

Data availability.

The Supplemental Information gives the description of the experimental setup of the MCBJ technique, calibration of the stretching rate and calculation of the snap-back distance by pure solvent, the original conductance measurement results of **OAE3**, **OAE4** and **OAE5**, the molecular junction angle geometry and the fitting for the master curve from the closing

process of OAE₂, the conductance-distance evolution for OAE₂, 3, 4 and 5, the evaluation of bias voltage and stretching rate, the super-exchange and hopping contribution calculation for OAE series, and the calculation of the through-molecule tunneling contributions in the OAE series. The data that support the findings of this study are available from the corresponding author upon reasonable request.

SUPPLEMENTAL INFORMATION

Supplemental Information includes 10 sections with 17 figures and can be found with this article online at <http://>

ACKNOWLEDGMENTS

This work was supported by the National Key R&D Program of China (2017YFA0204902). This work was also generously supported by Young Thousand Talent Project of China, the EC FP7 ITN 'MOLESCO' project number 606728, the National Natural Science Foundation of China (Nos. 21703188, 21673195, 21503179) and China Postdoctoral Science Foundation (2017M622060).

AUTHOR CONTRIBUTIONS

W.H. originally conceived the concept and designed the experiments. W. H., M. R. B. and Y. Y. co-supervised the project. J.L., Y.Y., M.R.B. and W.H. prepared the manuscript using feedback from other authors. Break-junction measurements were carried out in the laboratory of W.H. by J.L., J.Z., F.W., X.H. and L.W.; MCBJ set-up was designed and realized by W.H, S.J., R.L. and J.L. in the laboratory of W.H.; Data analyses were carried out by J. L. with the assistance of Y.T., C.H. and W.H.. Synthetic works of the OAE molecules were carried out in the laboratory of M.R.B. by X.Z. All authors have given approval to the final version of the manuscript.

DECLARATION OF INTERESTS

The authors declare no competing interests.

REFERENCES AND NOTES

1. Wu, B., and Kumar, A. (2014). Extreme ultraviolet lithography and three dimensional integrated circuit-a review. *Appl. Phys. Rev.* *1*, 011104.
2. DeBenedictis, E.P. (2017). It's time to redefine Moore's law again. *Computer* *50*, 72-75.
3. Walter, M.W., and Thomas, M. (2017). Silicon and germanium nanowire electronics: Physics of conventional and unconventional transistors. *Rep. Prog. Phys.* *80*, 066502.
4. Mitchell, W.M. (2016). The chips are down for Moore's law. *Nature* *530*, 145-147.
5. Khan, H.N., Hounshell, D.A., and Fuchs, E.R.H. (2018). Science and research policy at the end of Moore's law. *Nature Electronics* *1*, 14-21.
6. Huang, C., Rudnev, A.V., Hong, W., and Wandlowski, T. (2015). Break junction under electrochemical gating: Testbed for single-molecule electronics. *Chem. Soc. Rev.* *44*, 889-901.
7. Perrin, M.L., Burzuri, E., and van der Zant, H.S.J. (2015). Single-molecule transistors. *Chem. Soc. Rev.* *44*, 902-919.
8. Su, T.A., Neupane, M., Steigerwald, M.L., Venkataraman, L., and Nuckolls, C. (2016). Chemical principles of single-molecule electronics. *Nat. Rev. Mater.* *1*, 16002.
9. Xiang, D., Wang, X., Jia, C., Lee, T., and Guo, X. (2016). Molecular-scale electronics: From concept to function. *Chem. Rev.* *116*, 4318-4440.
10. Xin, N., and Guo, X. (2017). Catalyst: The renaissance of molecular electronics. *Chem* *3*, 373-376.
11. Lörtscher, E. (2017). Reaction: Technological aspects of molecular electronics. *Chem* *3*, 376-377.
12. Puebla-Hellmann, G., Venkatesan, K., Mayor, M., and Lörtscher, E. (2018). Metallic nanoparticle contacts for high-yield, ambient-stable molecular-monolayer devices. *Nature* *559*, 232-235.
13. Schwarz, F., Kastlunger, G., Lissel, F., Egler-Lucas, C., Semenov, S.N., Venkatesan, K., Berke, H., Stadler, R., and Lörtscher, E. (2016). Field-induced conductance switching by charge-state alternation in organometallic single-molecule junctions. *Nat. Nanotechnol.* *11*, 170-176.
14. Jia, C., Migliore, A., Xin, N., Huang, S., Wang, J., Yang, Q., Wang, S., Chen, H., Wang, D., Feng, B., *et al.* (2016). Covalently bonded single-molecule junctions with stable and reversible photoswitched conductivity. *Science* *352*, 1443.
15. Chen, X., Roemer, M., Yuan, L., Du, W., Thompson, D., del Barco, E., and Nijhuis, C.A. (2017). Molecular diodes with rectification ratios exceeding 105 driven by electrostatic interactions. *Nat. Nanotechnol.* *12*, 797-803.
16. Atesci, H., Kaliginedi, V., Celis Gil, J.A., Ozawa, H., Thijssen, J.M., Broekmann, P., Haga, M.-a., and van der Molen, S.J. (2018). Humidity-controlled rectification switching in ruthenium-complex molecular junctions. *Nat. Nanotechnol.* *13*, 117-121.
17. Gotsmann, B., Riel, H., and Lörtscher, E. (2011). Direct electrode-electrode tunneling in break-junction measurements of molecular conductance. *Phys. Rev. B* *84*, 205408.

18. Quan, R., Pfitter, C.S., Ratner, M.A., and Reuter, M.G. (2015). Quantitative interpretations of break junction conductance histograms in molecular electron transport. *ACS Nano* **9**, 7704-7713.
19. Choi, S., Kim, B., and Frisbie, C.D. (2008). Electrical resistance of long conjugated molecular wires. *Science* **320**, 1482-1486.
20. Hines, T., Diez-Perez, I., Hihath, J., Liu, H., Wang, Z.-S., Zhao, J., Zhou, G., Müllen, K., and Tao, N. (2010). Transition from tunneling to hopping in single molecular junctions by measuring length and temperature dependence. *J. Am. Chem. Soc.* **132**, 11658-11664.
21. Zhao, X., Huang, C., Gulcur, M., Batsanov, A.S., Baghernejad, M., Hong, W., Bryce, M.R., and Wandlowski, T. (2013). Oligo(aryleneethynylene)s with terminal pyridyl groups: Synthesis and length dependence of the tunneling-to-hopping transition of single-molecule conductances. *Chem. Mater.* **25**, 4340-4347.
22. Haiss, W., Wang, C., Grace, I., Batsanov, A.S., Schiffrin, D.J., Higgins, S.J., Bryce, M.R., Lambert, C.J., and Nichols, R.J. (2006). Precision control of single-molecule electrical junctions. *Nat. Mater.* **5**, 995-1002.
23. Quek, S.Y., Kamenetska, M., Steigerwald, M.L., Choi, H.J., Louie, S.G., Hybertsen, M.S., Neaton, J.B., and Venkataraman, L. (2009). Mechanically controlled binary conductance switching of a single-molecule junction. *Nat. Nanotechnol.* **4**, 230-234.
24. Hong, W., Manrique, D.Z., Moreno-García, P., Gulcur, M., Mishchenko, A., Lambert, C.J., Bryce, M.R., and Wandlowski, T. (2012). Single molecular conductance of tolans: Experimental and theoretical study on the junction evolution dependent on the anchoring group. *J. Am. Chem. Soc.* **134**, 2292-2304.
25. Aradhya, S.V., Frei, M., Hybertsen, M.S., and Venkataraman, L. (2012). Van der waals interactions at metal/organic interfaces at the single-molecule level. *Nat. Mater.* **11**, 872-876.
26. Reed, M.A., Zhou, C., Muller, C.J., Burgin, T.P., and Tour, J.M. (1997). Conductance of a molecular junction. *Science* **278**, 252-254.
27. Wu, S., Gonzalez, M.T., Huber, R., Grunder, S., Mayor, M., Schonenberger, C., and Calame, M. (2008). Molecular junctions based on aromatic coupling. *Nat. Nanotechnol.* **3**, 569-574.
28. Kim, Y., Song, H., Strigl, F., Pernau, H.-F., Lee, T., and Scheer, E. (2011). Conductance and vibrational states of single-molecule junctions controlled by mechanical stretching and material variation. *Phys. Rev. Lett.* **106**, 196804.
29. Manrique, D.Z., Huang, C., Baghernejad, M., Zhao, X., Al-Owaedi, O.A., Sadeghi, H., Kaliginedi, V., Hong, W., Gulcur, M., Wandlowski, T., *et al.* (2015). A quantum circuit rule for interference effects in single-molecule electrical junctions. *Nat. Commun.* **6**, 6389.
30. Frisenda, R., Janssen, V.A.E.C., Grozema, F.C., van der Zant, H.S.J., and Renaud, N. (2016). Mechanically controlled quantum interference in individual π -stacked dimers. *Nat. Chem.* **8**, 1099-1104.
31. Tour, J.M. (2000). Molecular electronics. Synthesis and testing of components. *Acc. Chem. Res.* **33**, 791-804.
32. Huber, R., González, M.T., Wu, S., Langer, M., Grunder, S., Horhoiu, V., Mayor, M., Bryce, M.R., Wang, C., Jitcathi, R., *et al.* (2008). Electrical conductance of conjugated oligomers at the single molecule level. *J. Am. Chem. Soc.* **130**, 1080-1084.
33. González, M.T., Zhao, X., Manrique, D.Z., Miguel, D., Leary, E., Gulcur, M., Batsanov, A.S., Rubio-Bollinger, G., Lambert, C.J., Bryce, M.R., *et al.* (2014). Structural versus electrical functionalization of oligo(phenylene ethynylene) diamine molecular junctions. *J. Phys. Chem. C* **118**, 21655-21662.
34. Hong, W., Valkenier, H., Mészáros, G., Manrique, D.Z., Mishchenko, A., Putz, A., García, P.M., Lambert, C.J., Hummelen, J.C., and Wandlowski, T. (2011). An MCBJ case study: The influence of π -conjugation on the single-molecule conductance at a solid/liquid interface. *Beilstein J. Nanotechnol.* **2**, 699-713.
35. Liu, J., Zhao, X., Al-Gailby, Q., Huang, X., Zheng, J., Li, R., Huang, C., Yang, Y., Shi, J., Manrique, D.Z., *et al.* (2017). Radical enhanced charge transport in single-molecule phenothiazine electrical junctions. *Angew. Chem. Int. Ed.* **56**, 13061-13065.
36. Balogh, Z., Visontai, D., Makk, P., Gillemot, K., Oroszlány, L., Pósa, L., Lambert, C., and Halbritter, A. (2014). Precursor configurations and post-rupture evolution of Ag-CO-Ag single-molecule junctions. *Nanoscale* **6**, 14784-14791.
37. Moreno-García, P., La Rosa, A., Koliwoška, V., Bermejo, D., Hong, W., Yoshida, K., Baghernejad, M., Filippone, S., Broekmann, P., Wandlowski, T., *et al.* (2015). Charge transport in c60-based dumbbell-type molecules: Mechanically induced switching between two distinct conductance states. *J. Am. Chem. Soc.* **137**, 2318-2327.
38. Yelin, T., Korytar, R., Sukenik, N., Vardimon, R., Kumar, B., Nuckolls, C., Evers, F., and Tal, O. (2016). Conductance saturation in a series of highly transmitting molecular junctions. *Nat. Mater.* **15**, 444-449.
39. Yanson, A.I., Bollinger, G.R., van den Brom, H.E., Agrait, N., and van Ruitenbeek, J.M. (1998). Formation and manipulation of a metallic wire of single gold atoms. *Nature* **395**, 783-785.
40. Kamenetska, M., Quek, S.Y., Whalley, A.C., Steigerwald, M.L., Choi, H.J., Louie, S.G., Nuckolls, C., Hybertsen, M.S., Neaton, J.B., and Venkataraman, L. (2010). Conductance and geometry of pyridine-linked single-molecule junctions. *J. Am. Chem. Soc.* **132**, 6817-6821.
41. González, M.T., Díaz, A., Leary, E., García, R., Herranz, M.Á., Rubio-Bollinger, G., Martín, N., and Agrait, N. (2013). Stability of single- and few-molecule junctions of conjugated diamines. *J. Am. Chem. Soc.* **135**, 5420-5426.
42. Kolb, D.M., Ullmann, R., and Will, T. (1997). Nanofabrication of small copper clusters on gold(111) electrodes by a scanning tunneling microscope. *Science* **275**, 1097.
43. Untiedt, C., Caturla, M.J., Calvo, M.R., Palacios, J.J., Segers, R.C., and van Ruitenbeek, J.M. (2007). Formation of a metallic contact: Jump to contact revisited. *Phys. Rev. Lett.* **98**, 206801.
44. Yang, Y., Liu, J., Feng, S., Wen, H., Tian, J., Zheng, J., Schöllhorn, B., Amatore, C., Chen, Z., and Tian, Z. (2016). Unexpected current-voltage characteristics of mechanically modulated atomic

contacts with the presence of molecular junctions in an electrochemically assisted-MCBI. *Nano Res.* **9**, 560-570.

45. Martin, C.A., Ding, D., Sørensen, J.K., Bjørnholm, T., van Ruitenbeek, J.M., and van der Zant, H.S.J. (2008). Fullerene-based anchoring groups for molecular electronics. *J. Am. Chem. Soc.* **130**, 13198-13199.

46. Untiedt, C., Yanson, A., Grande, R., Rubio-Bollinger, G., Agrait, N., Vieira, S., and van Ruitenbeek, J.M. (2002). Calibration of the length of a chain of single gold atoms. *Phys. Rev. B* **66**, 085418.

47. Huisman, E.H., Guédon, C.M., van Wees, B.J., and van der Molen, S.J. (2009). Interpretation of transition voltage spectroscopy. *Nano Lett.* **9**, 3909-3913.

48. Ittah, N., Yutsis, I., and Selzer, Y. (2008). Fabrication of highly stable configurable metal quantum point contacts. *Nano Lett.* **8**, 3922-3927.

49. Diez-Perez, I., Hihath, J., Hines, T., Wang, Z.-S., Zhou, G., Mullen, K., and Tao, N. (2011). Controlling single-molecule conductance through lateral coupling of $[\pi]$ orbitals. *Nat. Nanotechnol.* **6**, 226-231.

50. Kornilovitch, P.E., and Bratkovsky, A.M. (2001). Orientational dependence of current through molecular films. *Phys. Rev. B* **64**, 195413.

51. Toyoda, K., Morimoto, K., and Morita, K. (2006). First-principles study on current through a single π conjugate molecule for analysis of carrier injection through an organic/metal interface. *Surf. Sci.* **600**, 5080-5083.

52. Frei, M., Aradhya, S.V., Koentopp, M., Hybertsen, M.S., and Venkataraman, L. (2011). Mechanics and chemistry: Single molecule bond rupture forces correlate with molecular backbone structure. *Nano Lett.* **11**, 1518-1523.

53. Huisman, E.H., Trouwborst, M.L., Bakker, F.L., de Boer, B., van Wees, B.J., and van der Molen, S.J. (2008). Stabilizing single atom contacts by molecular bridge formation. *Nano Lett.* **8**, 3381-3385.

54. Huang, C., Jevric, M., Borges, A., Olsen, S.T., Hamill, J.M., Zheng, J.-T., Yang, Y., Rudnev, A., Baghernejad, M., Broekmann, P., *et al.* (2017). Single-molecule detection of dihydroazulene photo-thermal reaction using break junction technique. *Nat. Commun.* **8**, 15436.

55. Garner, M.H., Li, H., Chen, Y., Su, T.A., Shangguan, Z., Paley, D.W., Liu, T., Ng, F., Li, H., Xiao, S., *et al.* (2018). Comprehensive suppression of single-molecule conductance using destructive σ -interference. *Nature* **558**, 415-419.

56. Vazquez, H., Skouta, R., Schneebeli, S., Kamenetska, M., Breslow, R., Venkataraman, L., and Hybertsen, M.S. (2012). Probing the conductance superposition law in single-molecule circuits with parallel paths. *Nat. Nanotechnol.* **7**, 663-667.

57. Ionescu, A.M., and Riel, H. (2011). Tunnel field-effect transistors as energy-efficient electronic switches. *Nature* **479**, 329-337.

FIGURE AND SCHEME TITLES AND LEGENDS

Figure 1. Schematic, technique and molecules used in this work. (A) The competition between the molecular conductance (molecular tunneling) and the tunneling leakage current (through-space tunneling) through the two-terminal system during charge transport in a single-molecular junction. (B) The MCBI method with gold electrodes immersed in a solution of targeted molecules. (C) The oligo(aryleneethynylene) (OAE) series of molecules adopted in this study. The numbers 2-5 refer to the number of ethynylphenylene units in OAE molecules, and OAE2 is used for example in (A) and (B).

Figure 2. Conductance measurements, master curve extracting and fitting of OAE2 molecule. (A) Typical conductance-distance curves of OAE2 recorded during the opening (blue) and closing (green) processes. (B) 1D conductance histograms constructed from the opening and closing processes. 2D conductance-distance histograms with master curves of the (C) opening and (D) closing processes. Lower left insets: the distance distribution determined from $10^{-1.0} G_0$ to $10^{-4.8} G_0$. (E) Superimposition of the opening (blue) and closing (green) master curves with the simulated dots (orange). The opening and simulated curves are aligned to the conductance drop after the molecular plateau. The black dash line labels the fitting of the through-space tunneling. The simulated data are from our previous report, reprinted with permission from ref. 24 Copyright 2012 American Chemical Society. (F) Non-linear fitting (orange curve) of the through-molecule tunneling regime of the master curve in closing process, top-z axis shows the corresponded estimated tilt angle of molecular junction, the part of molecular junction break into background are omitted.

Figure 3. Conductance measurements and relative displacement distributions of the OAE series. The 2D conductance-distance histograms of the closing process with master curves extracted for (A) OAE3, (B) OAE4, (C) OAE5. (D) The relative displacement distributions of OAE series in opening and closing processes. The conductance ranges to determine the distances were from $10^{-1.0}$ to $10^{-4.8} G_0$, $10^{-1.0}$ to $10^{-6.0} G_0$, $10^{-1.0}$ to $10^{-6.8} G_0$ and $10^{-1.0}$ to $10^{-8.0} G_0$ for OAE2, 3, 4 and 5, respectively. (E) The distance distributions in each process versus molecular length, which is plotted against the number of aryl rings in the OAE series (For the molecular length values, see Table 1). The orange dash line represents the equality between molecular lengths of OAE series and calibrated distance of closing process.

Figure 4. The transition between the through-space tunneling and molecular tunneling. (A) Left plot: the master curves of the OAE series are superimposed for comparison. The direct tunneling regime as tunneling background is fitted through the black dash line, the molecular tunneling

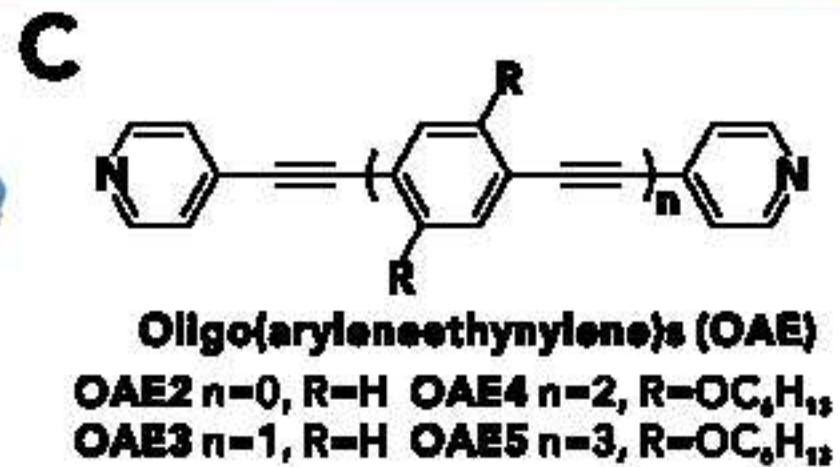
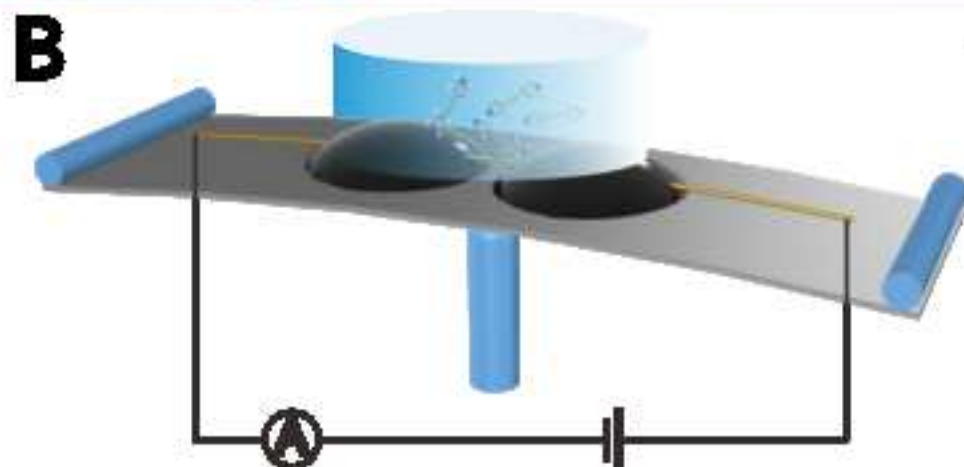
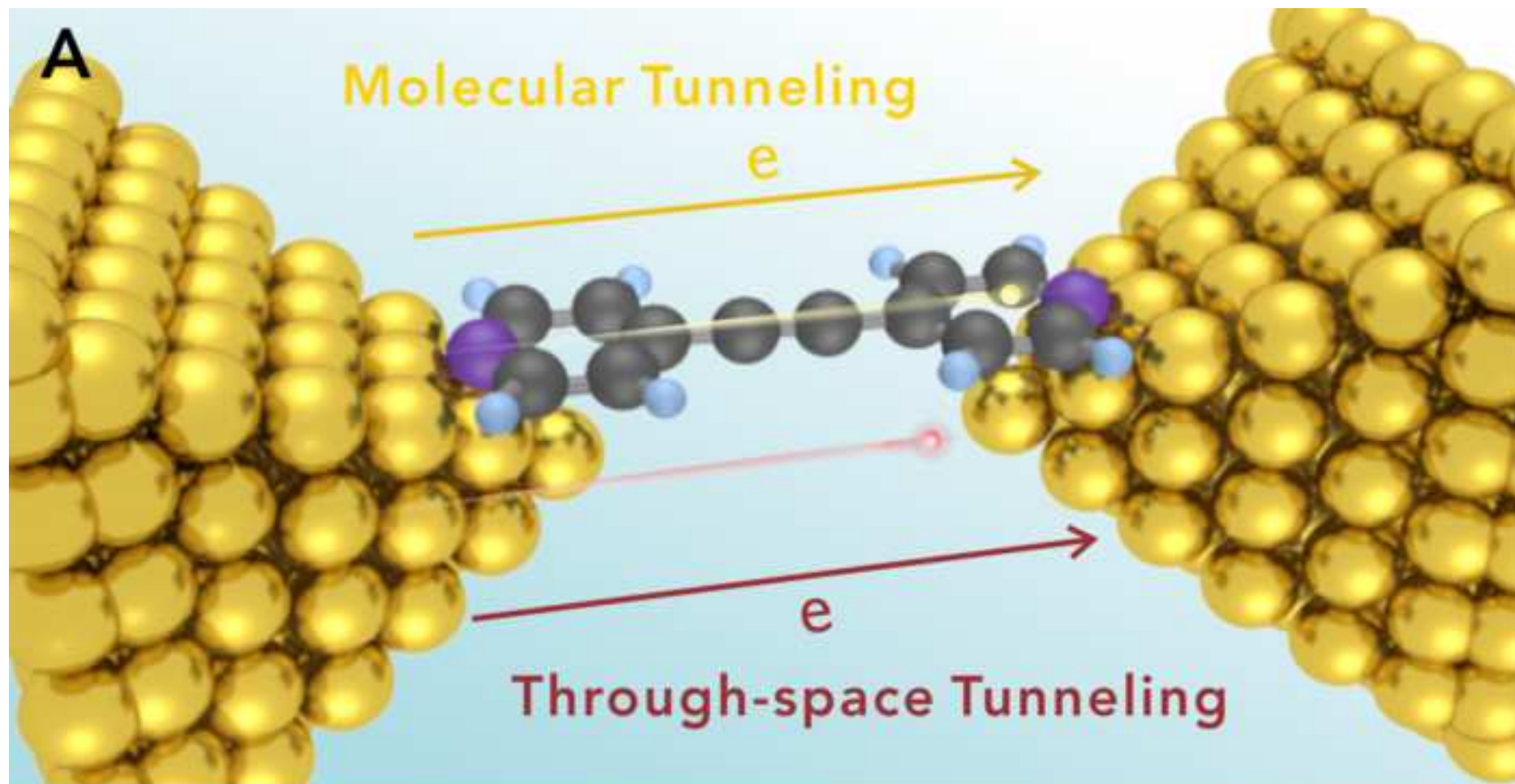
regime was fitted by non-linear fitting through the orange solid line. Right plot: the 1D conductance histograms constructed from 1000 curves for each molecule, where all the peak heights are normalized. (B) The transition distance describes the transition from molecular tunneling to through-space tunneling process for each **OAE** molecules, which is plotted against the molecular lengths of the **OAE** series. (For the transition distance values, see Table 1).

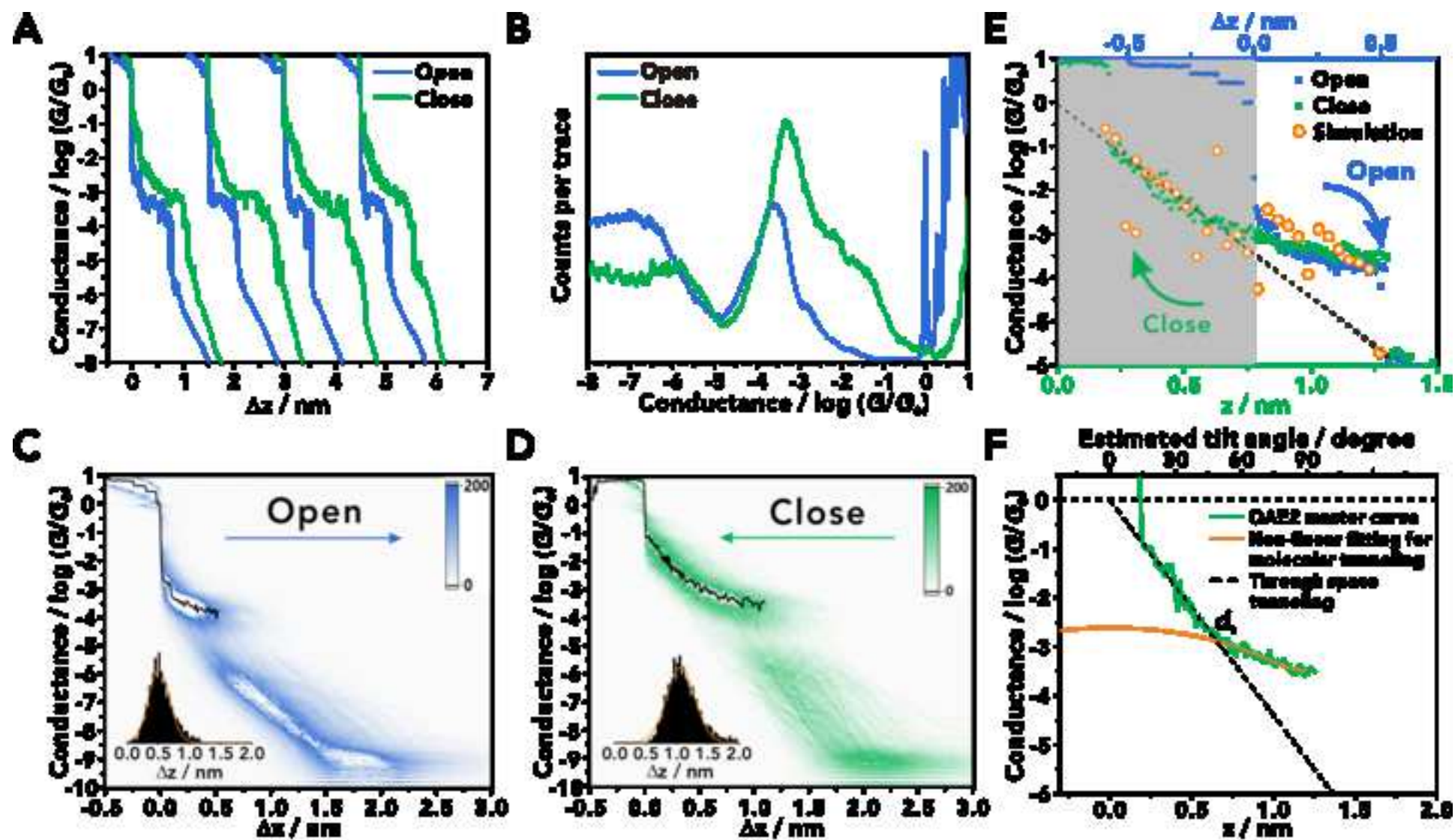
TABLES AND TABLE TITLES AND LEGENDS

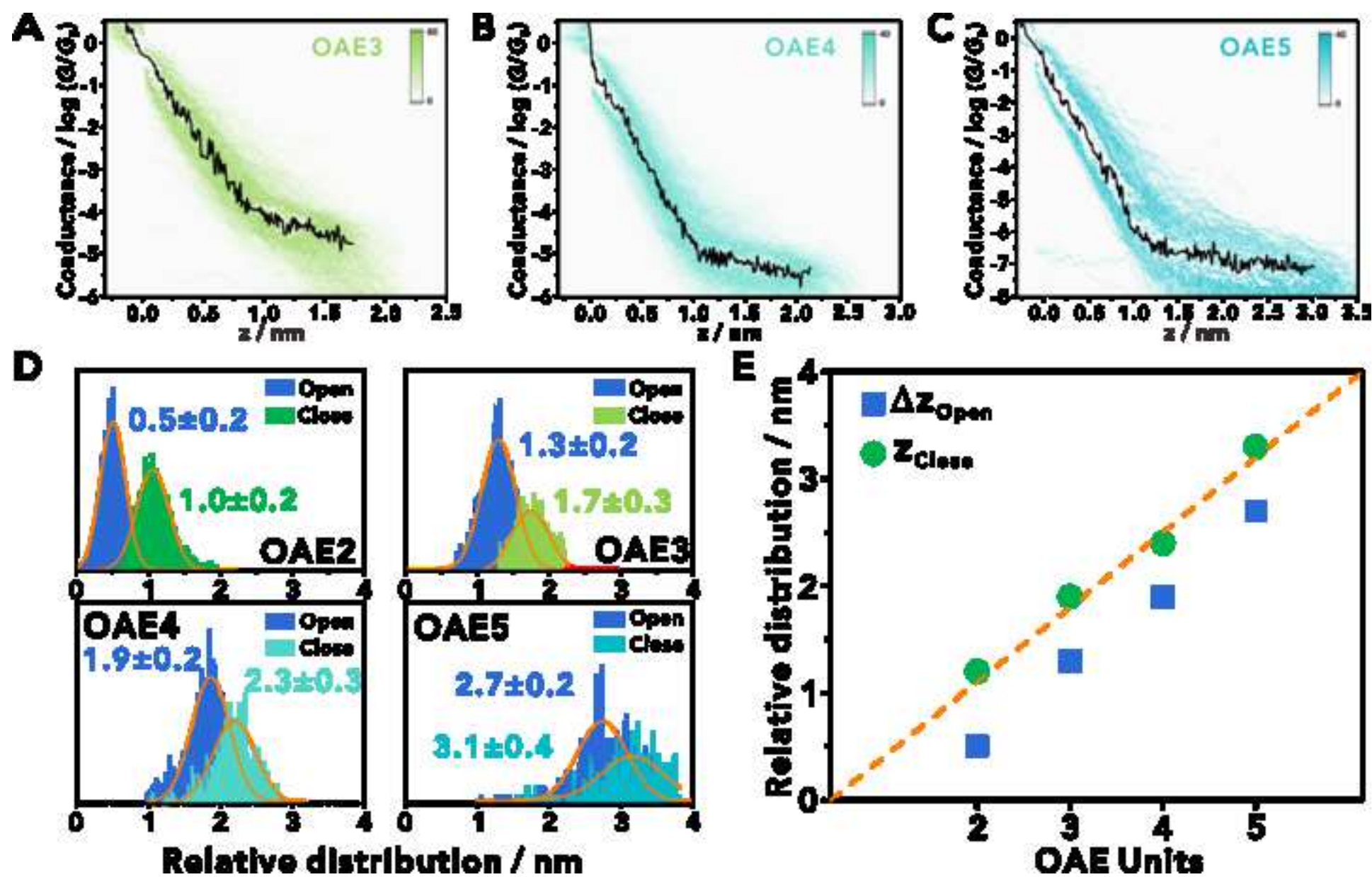
Table 1. The measured charge transport results and the calculated transition distance of OAE series. The measured conductance and length of different processes for OAE series, compared with molecular length by calibration. The calculation of the transition distance from through-space tunneling regime to molecular tunneling regime, and the calculated tilted angle of the molecular junction at the transition distance.

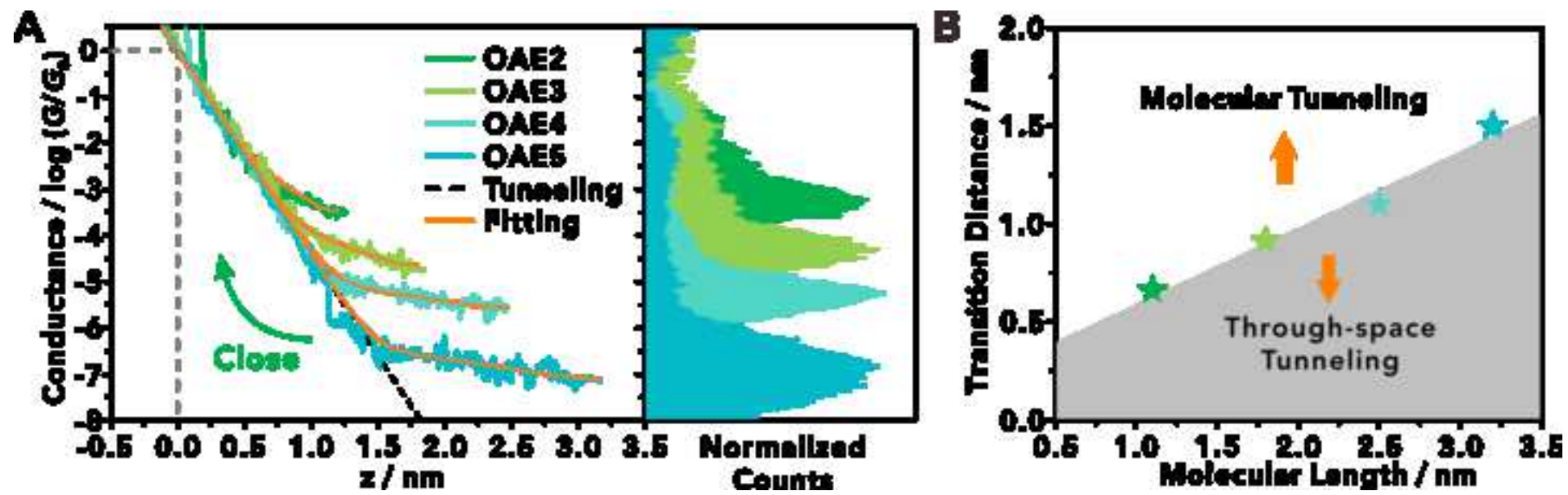
Molecule	Conductance / $\log(G/G_0)$		Molecular Length / nm	Δz_{Open} / nm	$\Delta z_{\text{Close}},$ d_m / nm	Transition Distance , d_t / nm	Tilted Angle, θ / degree
	Open	Close					
OAE2	-3.6 ± 0.3	-3.2 ± 0.3	1.1	0.5 ± 0.2	1.2 ± 0.2	0.66	35.1
OAE3	-4.6 ± 0.3	-4.3 ± 0.4	1.8	1.3 ± 0.3	1.9 ± 0.3	0.91	31.4
OAE4	-5.8 ± 0.3	-5.3 ± 0.4	2.5	1.9 ± 0.3	2.5 ± 0.3	1.2	28.7
OAE5	-7.0 ± 0.3	-7.0 ± 0.5	3.2	2.7 ± 0.4	3.3 ± 0.4	1.5	27.0

The conductance histograms of **OAE3**, **OAE4** and **OAE5** for the opening processes are shown in Supplemental Information Figures S3 to S5. The calibration in pure solvent and the absolute distance and the calculation of the transition distance are discussed in Supplemental Information 2, 4 and 5, respectively. Error bars are determined from the standard deviation in Gaussian fitting of conductance and length distribution.









Supporting Information: Table of Contents:

1. The experimental setup of MCBJ technique.
2. Calibration of the stretching rate and calculation of the snap-back distance by pure solvent.
3. The original conductance measurement results of **OAE3**, **OAE4** and **OAE5**.
4. Molecular junction angle geometry and the non-linear fitting for the master curve from the closing process of **OAE2**.
5. The conductance-distance evolution for the **OAE2**, **3**, **4** and **5**.
6. The conductance measurements of **OAE2** under different stretching rates.
7. The conductance measurements of **OAE2** under different bias voltages.
8. Super-exchange and hopping contribution calculation for the **OAE** series.
9. Calculation of the through-molecule tunneling contributions of the **OAE** series.
10. The transition in other conjugated systems.

1. The experimental setup of the MCBJ technique

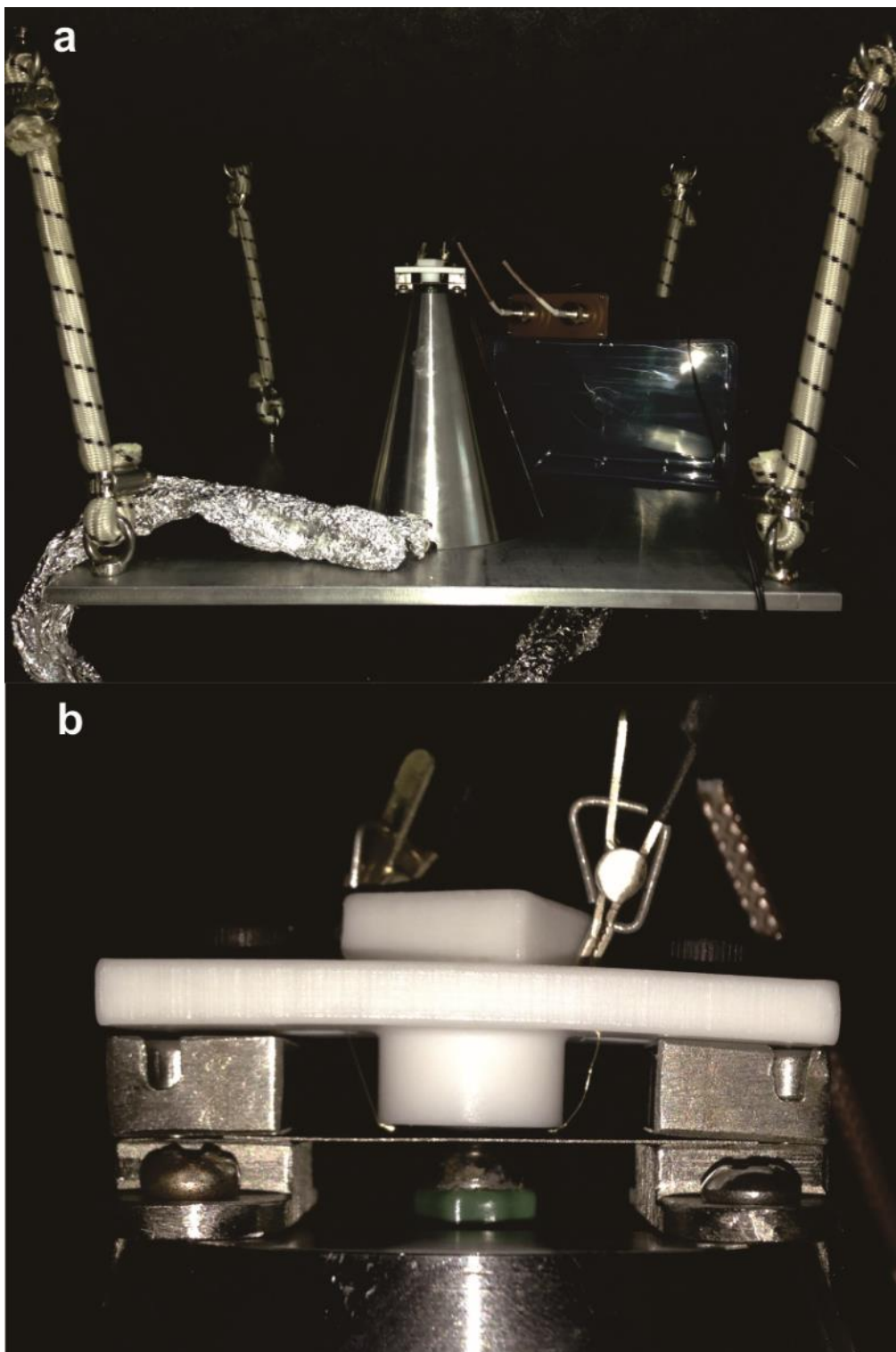


Figure S1. Schematic of (a) MCBJ setup and (b) the zoom-in image of the chip position.

2. Calibration of the stretching rate and calculation of the snap-back distance in pure solvent of THF/TMB.

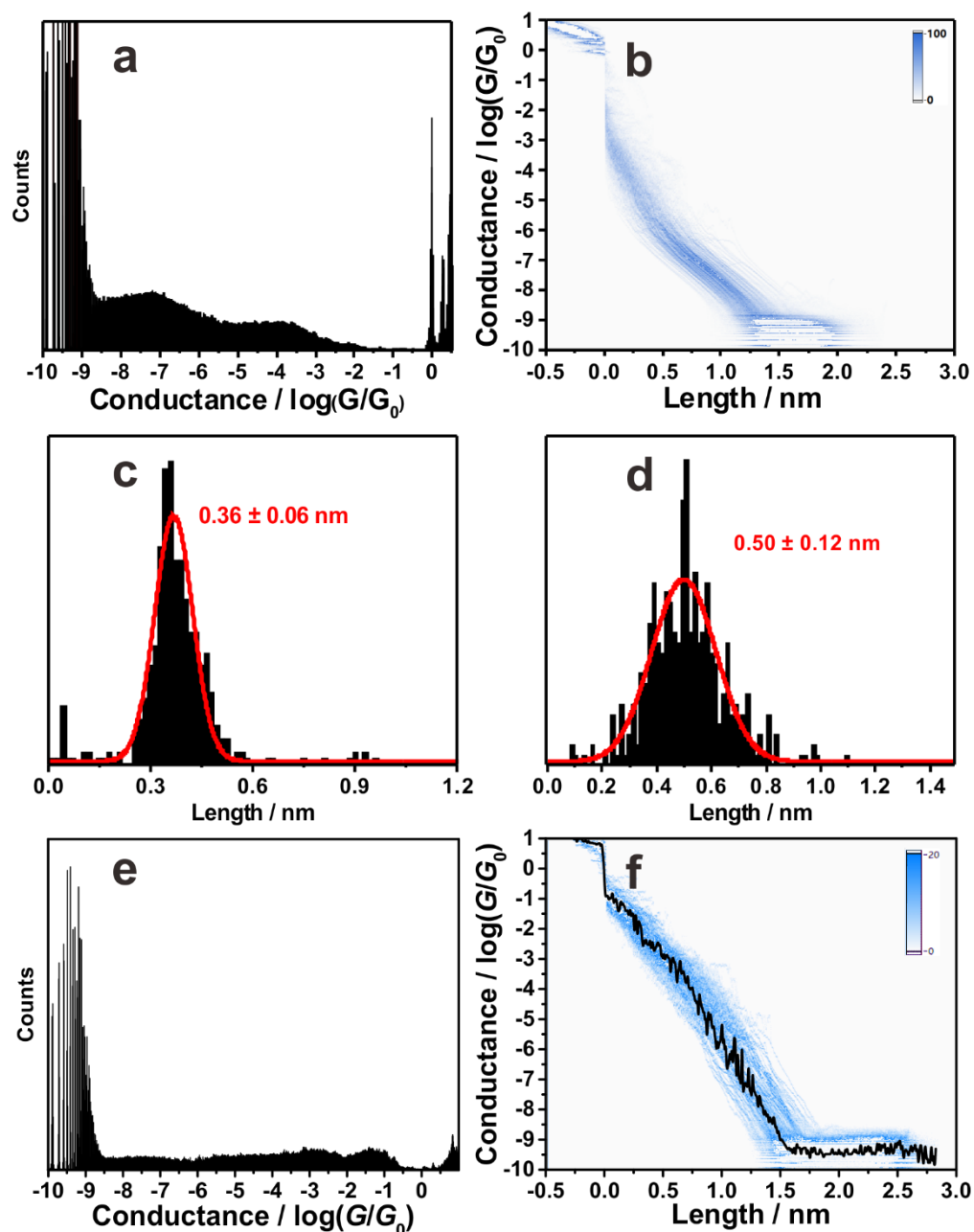


Figure S2. (a) 1D conductance histogram of the opening process in pure solvent (1:4 v/v THF:TMB). (b) 2D conductance-distance histogram of pure solvent. Characteristic length distribution (c) from $10^{-4.0} G_0$ to $10^{-6.0} G_0$ and (d) from $10^{-0.3} G_0$ to $10^{-6.0} G_0$ in a blank experiment. (e) 1D conductance histogram of the closing process in pure solvent. (f) 2D conductance-distance histogram of pure solvent with the extracted master curve.

We used the same method described elsewhere previously to calibrate the stretching rate of the electrode pair in pure solvent.^{1,2} Without the target molecule, the 1D conductance histogram and 2D conductance-distance histogram in Figure S2(a) and S2(b) show direct tunneling and clear non-plateau features, suggesting a pure and clean environment inside the gap. In order to calculate the snap-back distance, firstly we needed to calibrate the stretching rate of the pulled electrodes pair.

Since the tunneling equation can be written as follows,

$$(1) \quad G = G_0 e^{-\beta_T \Delta z}$$

Where β_T is the tunneling decay constant in the solution environment, Δz is the absolute distance, herein $\Delta z = z - z_{\text{corr}}$, where z_{corr} is the snap-back distance. Equation (1) can be transferred as follows when taking the logarithm of each side,

$$(2) \quad \log\left(\frac{G}{G_0}\right) = -0.434\beta_T(z - z_{\text{corr}})$$

Then a plot of $\log(G/G_0)$ versus z has a slope of $-0.434\beta_T$ and an intercept of $0.434\beta_T z_{\text{corr}}$, therefore, we can use the plot to get β_T and z_{corr} . As we had calibrated the tunneling decay constant under the liquid atmosphere of THF:TMB (v/v 1:4) and already obtained the slope as $\log[\Delta G/G_0]/\Delta z = -5.5 \text{ nm}^{-1}$,² for the tunneling conductance range from $10^{-4.0}$ to $10^{-6.0} G_0$, Δz should be 0.36 nm.

Hence, we calibrated the length histogram between $10^{-4.0}$ to $10^{-6.0} G_0$ to fit the Δz for 0.36 nm, as shown in Figure S2(c). As a consequence, the plot will extend to an intercept of 2.75, the z_{corr} will be $2.75/5.5 = 0.5 \text{ nm}$. Therefore, when the plateau length statistical range extends to between $10^{-0.3}$ (extend to the intercept) to $10^{-6.0} G_0$, it will be 0.5 nm, as shown in Figure S2(d), which is the snap-back distance close to the previous report. The stretching and approaching rate of electrodes pair was calculated to be $\sim 8.4 \text{ nm/s}$.

Moreover, we extracted the conductance evolution of the closing process in the pure solvent. Figure S2(e) and S2(f) shows the corresponding 1D and 2D conductance histograms with the extracted master curve. The through-space tunneling regime ranges from $10^{-1} G_0$ to even down to the scale of $10^{-8} G_0$, which demonstrated that the electron can tunnel between the face-to-face electrodes through a very long range. The small peak at around $10^{-1} G_0$ is in Figure S2(e) originated from the "jump-to-contact" process when the electrodes gap was too small that the electrodes will easily form contact. The fitted slope of the range from 10^{-1} to $10^{-8} G_0$ is 5.33 nm^{-1} , which is very close to the slope of the opening process (5.5 nm^{-1}), suggesting that the closing process is able to obtain the whole range of the conductance evolution. Besides, this pure tunneling character demonstrates a clean gold surface without contaminations adsorbed in the closing process, which enables further investigation with solution of target molecule.

3. The original conductance measurement results of **OAE3**, **OAE4** and **OAE5**.

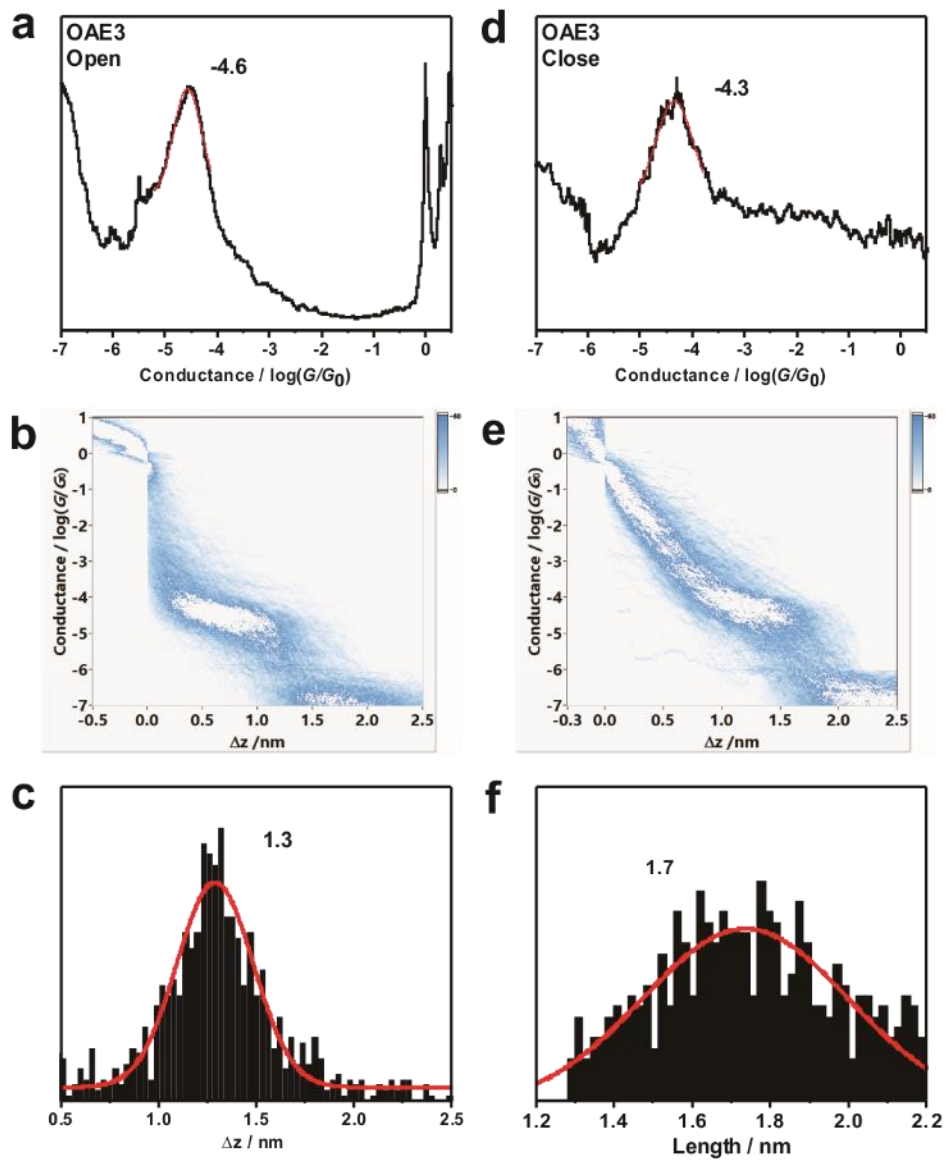


Figure S3. 1D conductance histogram of opening (a) and closing (d) processes, 2D conductance-distance histogram of opening (b) and closing (e) processes of **OAE3**. Plateau length histograms of stretch (c) and relax (f) processes, for both the analysis range is from $10^{-0.3}$ to $10^{-6.0} G_0$.

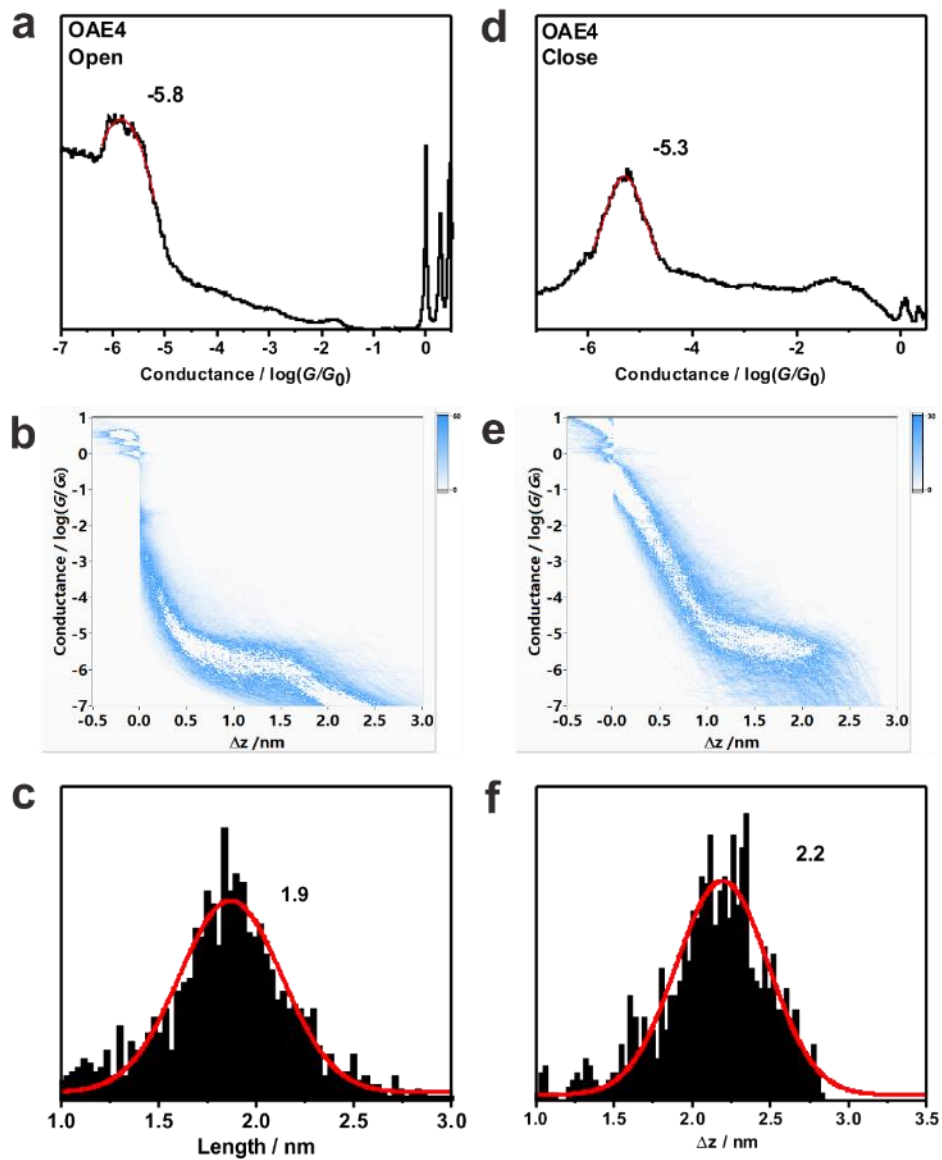


Figure S4. 1D conductance histogram of opening (a) and closing (d) processes, 2D conductance-distance histograms of opening (b) and closing (e) processes of **OAE4**. Plateau length histograms of stretch (c) and relax (f) processes, for both the analysis range is from $10^{-0.3}$ to $10^{-6.8} G_0$.

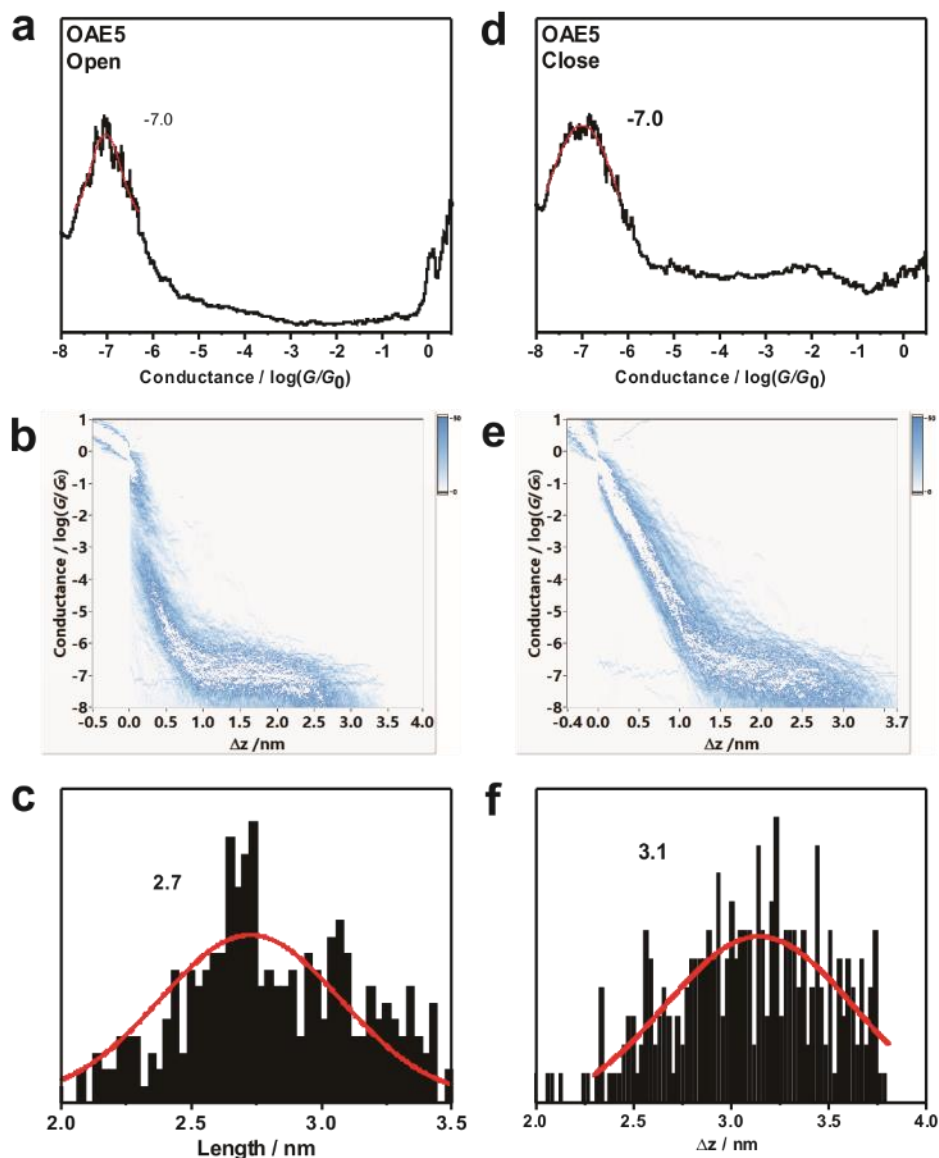


Figure S5. 1D conductance histograms of opening (a) and closing (d) processes, 2D conductance-distance histogram of opening (b) and closing (e) of **OAE5** molecule. Plateau length histogram of stretch (c) and relax (f) processes, for both the analysis range is from $10^{-0.3}$ to $10^{-8.0} G_0$.

4. Molecular junction angle geometry and fitting for the master curve from the closing process of **OAE2**.

As we had calibrated the stretching rate to obtain the snap-back distance, we used the same system and operational parameters for molecular conductance measurements, by replacing the pure solvent with 0.1 mM target molecule solution in the same solvent. Figure S6 shows the master curve extracted from the 2D conductance-distance histogram of the closing process of

OAE2. The prominent different regime suggests the different major contribution between through-space tunneling and through molecule tunneling.

A jump-to-contact process is observed at the conductance of about $10^{-0.78} G_0$, which is similar to previous results.³ Therefore, the logarithmic conductance evolved linearly with the electrode distance, we used the linear fitting over the range of -1.0 to -3.0 $\log(G/G_0)$, and found the slope is -4.393. According to equation (2), the β_T in the molecular solution will be

$$(3) \quad \beta_T = -4.393 / -0.434 = 10 \text{ nm}^{-1}$$

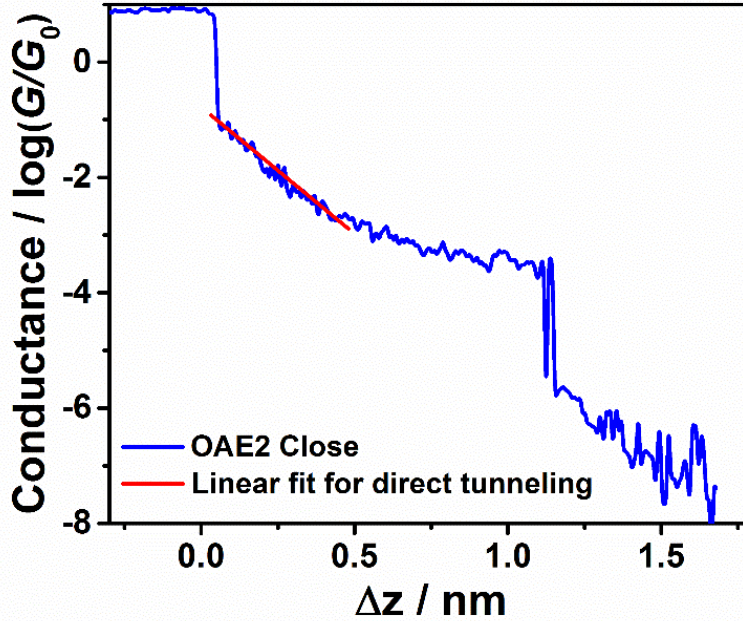


Figure S6. The master curve extracted from 2D conductance-distance histogram of closing process of **OAE2**, with red linear fitting for through-space tunneling regime.

Although there is a slight difference of the β_T between the pure solvent ($-5.5/-0.434 = 12 \text{ nm}^{-1}$) and the **OAE** solution, which can be attributed to the change of tunneling barrier because of the molecular adsorption,⁴ we considered that the β_T in the molecular solution was entirely reasonable.

Furthermore, through the fitting, as shown in Figure S6, the tunneling equation will be

$$(4) \quad \log\left(\frac{G}{G_0}\right) = -4.393\Delta z - 0.7801$$

Therefore, in order to calibrate the absolute distance, we set Δz equals to $z + \Delta d$. Δd is the calibrated distance between the z axis of the previous obtained master curve in Figure S6 and the calibrated z axis. It is known that when z equals to 0, G equals to G_0 , which means the gold atomic contact forms. Therefore, we obtained

$$(5) \quad \log\left(\frac{G}{G_0}\right) = \log\left(\frac{G_0}{G_0}\right) = -4.393z + 4.393\Delta d - 0.7801 = 0$$

Then the Δd will be

$$(6) \quad \Delta d = 0.177 \text{ nm}$$

Hence, we calibrated all the closing master curves by adding Δd in the z axis, as shown in Figure 2E, 2F and Figure 4A in the main text. The tunneling G_t , the equation (5) ($\log(G_t/G_0) = -4.393z$) was also plotted as a black dash line in Figure 2E, 2F and Figure 4A.

Therefore, the closing process and the corresponding opening process can be described as follows in Figure S7, which indicates the junction evolution during the opening/closing processes. The blue curve indicates the stretching of a molecular junction from the configuration a to f , while the closing process exhibited a reverse sequence. Among those configurations, a represents multiple gold atomic contacts when the electrodes pair join together, while b represents a single-atom contact with the conductance of $1 G_0$. The configurations e and f , represent the most extended molecular junction and the molecular junction breakage, respectively. Therefore, configurations from c to d suggest the formed molecular junction with tilted configurations. Hence, as shown in the green curve of the closing process, the molecule adsorbed on the end of one electrode starts to contact with the end of the other electrode from the configuration f to e , during which the conductance might exhibit a jump from background to a conductance plateau. As the two electrodes approach closer, the distance becomes smaller than the molecular length, and the molecular junction starts to tilt from configuration e to c . During this process, the overall conductance becomes larger, the through-space tunneling becomes inevitable and starts to dominate at the configuration d . The further approaching causes the conductance jumps from 10^{-1} to $10^0 G_0$, where a jump-to-contact process occurs to make two gold electrodes contact, and the conductance quickly changes to above G_0 , as shown in configuration a . In the opening process, due to the fast snap-back of gold electrodes, the opening process evolves directly from single gold atomic contact of configuration b to configuration d , some parts or even the whole series of configuration c might be missing. In the closing process, since the snap-back effect can be avoided, it enables the full detection of the series configurations c , but without the single gold atomic contact of configuration b .

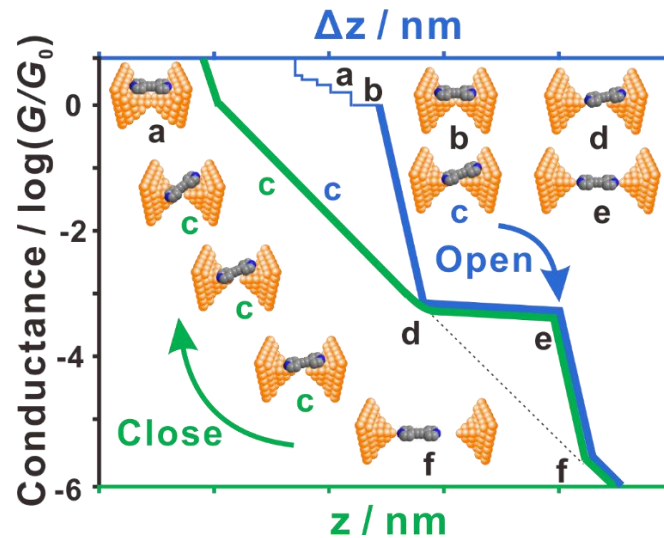


Figure S7. The hypothesized evolution of the molecular configuration during the opening and closing processes.

While in another part of the closing master curve of **OAE2**, the conductance plateau represents the through-molecule tunneling, according to the previous reports.⁵⁻⁷ The conductance of π -conjugated molecular junctions in the non-resonant tunneling regime will significantly correlate with the adsorption angle θ between the conjugated backbone and the electrode surface, especially for the large delocalized rigid conjugated molecular systems, where it is predicted that the conductance $G \propto \cos^4\theta$. Figure S8 shows the junction geometry changes of the short **OAE2** and long **OAE5** (the OC_6H_{13} side groups are omitted) as examples. Therefore, θ can be estimated by the arcsine of z/d_m , where z is the absolute electrode distance calibrated as discussed above, d_m is the molecular length. For the Au-pyridyl contacts, the correlation between the conductance variation with the tilt angle mainly originates from the coupling between the lateral π -orbital and the gold electrode. Since the tilted angle correlates with the electrode distance, the distance changes will lead to the conductance change due to the tilted angle variation. As the possible sliding of Au-pyridyl contact did not cause the changes of the angle, the molecular conductance change may be quite small since the target molecules we used are long, rigid backbones with lateral π -orbitals, therefore, the conductance changes were dominated by the changes of the tilt angles during the break junction process.

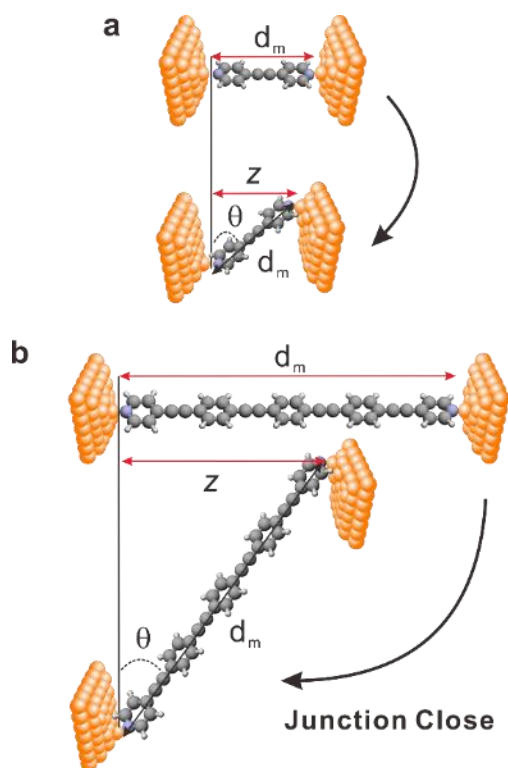


Figure S8. Schematics of junction geometries when the molecule is fully extended (upper panels) and tilted with an angle θ (lower panels) for (a) **OAE2** and (b) **OAE5**, d_m is the molecular length and z is the electrode distance.

Therefore, in order to establish the relationship between the electrode distance and the molecular conductance G_m , the master curve was fitted with equation (7) below

$$(7) \quad \log\left(\frac{G_m}{G_0}\right) = \log\left\{A \left[\cos\left(\arcsin\left(\frac{z}{d_m}\right)\right)\right]^n + B\right\}$$

where we used A, B, n as fitting parameters. A means the pre-factor where ref. 5 suggested $A \cdot G_0$ equals $e^2/h \cdot \Gamma^2/t_\pi^2$, Γ stands for the coupling between molecule and the gold electrode, and t_π correlates with the energy difference between HOMO-LUMO gap of molecule. While $B \cdot G_0$ is the molecular conductance when the molecular junction is fully extended when the angle reaches 90 degree (configuration e in Figure S7). For n, it supposed to be 4 according to the ref. 5, however since the junction evolves under room temperature and solution phase, the molecular level broadening and the coupling between molecule and electrode will be different, causing the actual circumstance different from the ideal theoretical assumption, it will be better to fit the n also. The d_m for **OAE2** is 1.2 nm, and the fitting range of z is from 0.7 to 1.2 nm for the molecular conductance plateau, as shown in Figure S9 and equation (8), the regression coefficient $r^2 = 0.9141$.

$$(8) \quad \log(G_m/G_0) = \log\{2.1 \times 10^{-3} [\cos(\arcsin(z/1.2))]^{4.3304} + 3.3288 \times 10^{-4}\}$$

Then the overall conductance G originates from the through-space tunneling conductance G_t and molecular tunneling conductance G_m by combining equation (5) with equation (8),

$$(9) \quad \log(G/G_0) = \log((G_t + G_m)/G_0) \\ = \log\{10^{-4.393z} + 2.1 \times 10^{-3} [\cos(\arcsin(z/1.2))]^{4.3304} + 3.3288 \times 10^{-4}\}$$

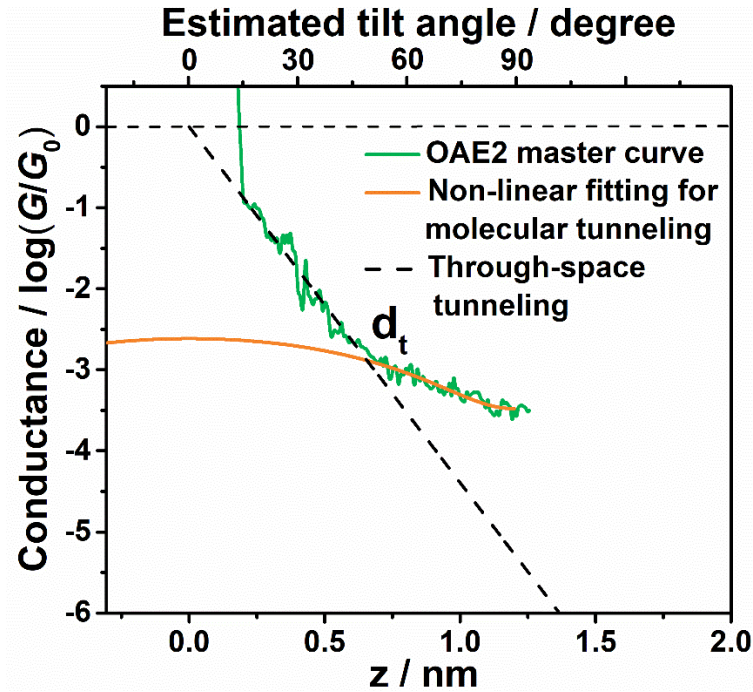


Figure S9. Non-linear fitting (orange curve) of the through-molecular tunneling regime of the master curve of the closing process. The top-z axis shows the corresponding estimated tilt angle of the molecular junction, the parts of the master curve where the molecular junction break into background are omitted.

Therefore, the intersection of the through-space tunneling and molecular tunneling will be

obtained by setting the equation (5) equal to equation (8), and the transition distance d_t will be about 0.66 nm, as shown in Figure S9.

5. The conductance-distance evolution for **OAE2**, **3**, **4** and **5**.

Furthermore, for other **OAE** molecules, the non-linear fitting of the molecular conductance plateau G_m was also conducted based on equation (7).

For **OAE3**, the molecular length is 1.9 nm, the fitting range of z is from 1.0 to 1.8 nm for the molecular conductance plateau, the r^2 is 0.9086.

$$(10) \quad \log\left(\frac{G_m}{G_0}\right) = \log\left\{1.5099 \times 10^{-4} [\cos(\arcsin(z/1.9))]^{4.5403} + 2.2712 \times 10^{-5}\right\}$$

Then the whole close curve of **OAE3** can be fitted as

$$(11) \quad \begin{aligned} \log\left(\frac{G}{G_0}\right) &= \log\left(\frac{(G_t + G_m)}{G_0}\right) \\ &= \log\left\{10^{-4.393z} + 1.5099 \times 10^{-4} [\cos(\arcsin(z/1.9))]^{4.5403} + 2.2712 \times 10^{-5}\right\} \end{aligned}$$

For **OAE4**, the molecular length is 2.5 nm, the fitting range of z is from 1.2 to 2.5 nm for the molecular conductance plateau, the r^2 is 0.8078.

$$(12) \quad \log\left(\frac{G_m}{G_0}\right) = \log\left\{8.3686 \times 10^{-6} [\cos(\arcsin(z/2.5))]^{4.1514} + 2.7518 \times 10^{-6}\right\}$$

Then the whole close curve of **OAE4** can be fitted as

$$(13) \quad \begin{aligned} \log\left(\frac{G}{G_0}\right) &= \log\left(\frac{(G_t + G_m)}{G_0}\right) \\ &= \log\left\{10^{-4.393z} + 8.3686 \times 10^{-6} [\cos(\arcsin(z/2.5))]^{4.1514} + 2.7518 \times 10^{-6}\right\} \end{aligned}$$

For **OAE5**, the molecular length is 3.3 nm, the fitting range of z is from 1.5 to 3.2 nm for the molecular conductance plateau, the r^2 is 0.8309.

$$(14) \quad \log\left(\frac{G_m}{G_0}\right) = \log\left\{3.8405 \times 10^{-7} [\cos(\arcsin(z/3.3))]^{4.2380} + 7.8576 \times 10^{-8}\right\}$$

Then the whole closing curve of **OAE5** can be fitted as

$$(15) \quad \begin{aligned} \log\left(\frac{G}{G_0}\right) &= \log\left(\frac{(G_t + G_m)}{G_0}\right) \\ &= \log\left\{10^{-4.393z} + 3.8405 \times 10^{-7} [\cos(\arcsin(z/3.3))]^{4.2380} + 7.8576 \times 10^{-8}\right\} \end{aligned}$$

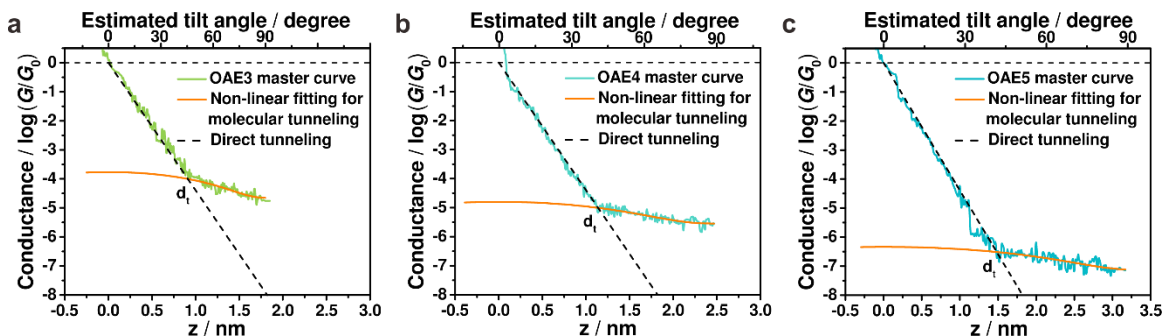


Figure S10. The master curves of the closing processes of (a) **OAE3** (b) **OAE4** and (c) **OAE5**, with orange lines for non-linear fittings of the through molecular tunneling regime, top- z axes show the corresponded estimated tilt angles of the molecule junctions, the parts of the master curve where the molecular junctions break into background are omitted.

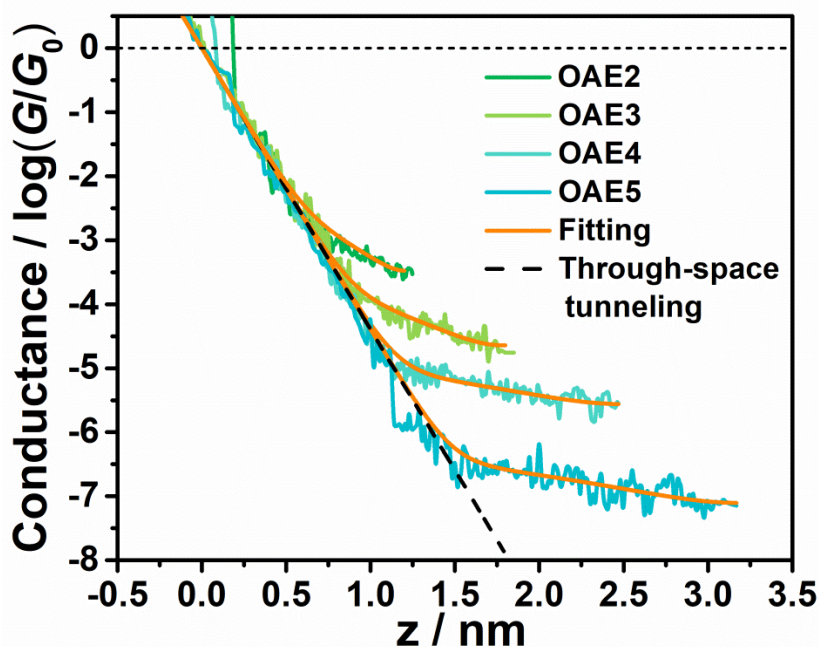


Figure S11. The superimposed master curves of the closing processes of **OAE** molecules, with orange lines for non-linear fittings of the through-molecular tunneling regime.

Therefore, we can also calibrate the absolute distance for the other three closing processes. The non-linear fitting, as mentioned above, was also conducted for the original extracted master curves of **OAE3** to **OAE5**, along with **OAE2**, which are shown as orange lines in Figure S10. Hence, as discussed for **OAE2**, the fitted molecular tunneling curve of other three **OAE** molecules will also cross over the through-space tunneling, and the transition points from molecular tunneling regime to through-space tunneling regime can be obtained for setting equations (10), (12) and (14) equals to equation (5), respectively, which are 0.91, 1.2 and 1.5 nm. In summary, the transition distances for **OAE2** to **OAE5** will be 0.66, 0.91, 1.2 and 1.5 nm, respectively, as shown in Table 1 in the main text.

Besides, the correlation between the absolute electrode distance and the overall conductance evolution was obtained. As a consequence, all the master curves from the closing processes of **OAE2** to **OAE5** were aligned at the original point according to the above discussion, and the fitted overall conductance evolution can be plotted by equations (9), (11), (13) and (15) for **OAE2** to **OAE5**, respectively, as shown in Figure S11 and Figure 4A in the main text. Interestingly, the slopes of the through-space tunneling regime of **OAE3** – **OAE5** molecules were almost the same as that of **OAE2**, suggesting that the β_T in the molecular solution was actually different from that in pure solvent, and moreover, the β_T is almost the same while using different **OAEs** self-assembled on gold surfaces.

6. The conductance measurements of OAE2 under different stretching rates

We have also tried different stretching rates of 6.9 nm/s and 14 nm/s using different samples. Both of the 2D conductance-distance histograms exhibited the same scenarios with two regimes of through-space tunneling and molecular tunneling. The master curves under those two stretching rates also show a prominent transition feature, as shown and summarized in Figure S12 below, the dash line indicates the transition point before adding the calibration distance. Therefore, we consider that different stretching rates have no influence on the conductance measurements.

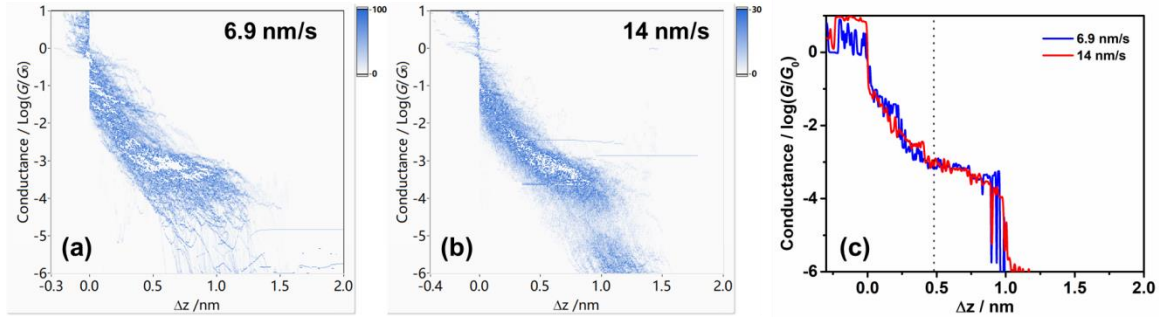


Figure S12. The conductance distance histograms of closing process under the electrodes approaching rate of (a) 6.9 nm/s and (b) 14 nm/s. The master curves extracted from both conditions were plotted together for comparison, the dash line indicates the transition between through-space tunneling and molecular tunneling.

7. The conductance measurements of OAE2 under different bias voltages.

The current of tunneling leakage will increase as the electric field increase. However, in our measurement, we used conductance values to provide more intrinsic properties. Nevertheless, we still need to evaluate the voltage dependence of the transition distance.

Further experiments on **OAE2** under different bias voltage are shown in Figure S13. The closing process under different bias also exhibited two regimes with through-space tunneling and molecular tunneling, which is the same as the phenomenon observed under bias voltage of 100 mV. After the same calibration process described in sections 4&5 in supplemental information, the fitting results are shown below:

For 50 mV, the molecular tunneling regime was fitted as plotted in orange line in Figure S13(a):

$$\log\left(\frac{G_m}{G_0}\right) = \log\left\{2.8 \times 10^{-3} [\cos(\arcsin(z/1.2))]^{4.0949} + 5.68 \times 10^{-4}\right\}$$

which the regression coefficient $r^2 = 0.9403$. The transition distance is 0.63 nm.

For 200 mV, the molecular tunneling regime was fitted as plotted in orange line in Figure S13(b):

$$\log\left(G_m/G_0\right) = \log\left\{3.2 \times 10^{-3}[\cos(\arcsin(z/1.2))]^{4.2267} + 5.94 \times 10^{-4}\right\}$$

which the regression coefficient $r^2 = 0.9573$. The transition distance is 0.62 nm.

For 300 mV, the molecular tunneling regime was fitted as plotted in orange line in Figure S13(c):

$$\log\left(G_m/G_0\right) = \log\left\{3.1 \times 10^{-3}[\cos(\arcsin(z/1.2))]^{4.1520} + 4.30 \times 10^{-4}\right\}$$

which the regression coefficient $r^2 = 0.9296$. The transition distance is 0.64 nm.

Since the transition distance obtained in our previous condition of 100 mV was 0.66 nm, the above calculated transition distances under other bias voltages were in accord with our prediction, which indicates that the transition between through-space tunneling and molecular tunneling is independent to the small bias voltage range.

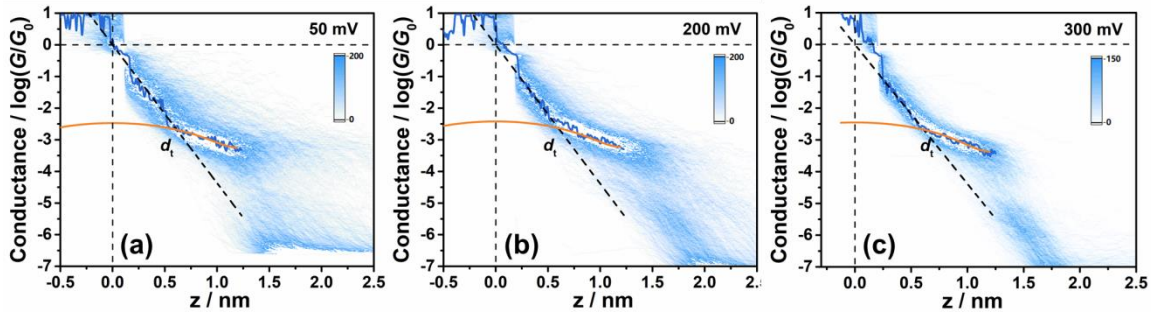


Figure S13. The calibrated closing processes with the corresponded 2D conductance-distance histograms under the bias voltage of (a) 50 mV, (b) 200 mV and (c) 300 mV. The orange line plotted on the master curve shows the fitting result of the molecular tunneling regime, while the tilt dash line shows the through-space tunneling regime.

Since our previous work had obtained the I - V properties of **OAE2** junction,¹ and the bias voltage of 100 mV in this work is relatively small and still locates at the linear area in the current-voltage curves of **OAE** molecular junctions, we considered the conductance features obtained are bias independent within the small bias range. Therefore, when using a small measuring voltage, the charge transport mechanism through molecular junction is still coherent tunneling, the transition distance might not be changed.

While for a much higher voltage, the Fowler-Nordheim tunneling will occur with increased conductance.⁸ Previous simulations suggested that as the electrodes gap becomes smaller, the transition voltage decreases,⁴ which means that as the gap decreases, it needs smaller bias voltage to evolve to the Fowler-Nordheim tunneling, thus much higher tunneling leakage will outstrip the intrinsic molecular tunneling when the electrodes approaching together. As a consequence, it will be earlier to reach the transition point from molecular tunneling to through-space tunneling during the closing process, causing a longer transition distance. However, since it needs high bias voltage (such as **OPE3-NH₂** the V_{trans} was reported to be 0.65 V)⁹ to realize the Fowler-Nordheim tunneling, the conductance measurement is difficult to be done because the molecular junction becomes rather unstable. Unfortunately, we cannot find obvious conductance

features under such high bias voltage. Nevertheless, it is of vital importance to confirm our assumption and we will make thorough investigations about the bias-dependent transition in future work.

8. Super-exchange and hopping contribution calculations for the OAE series.

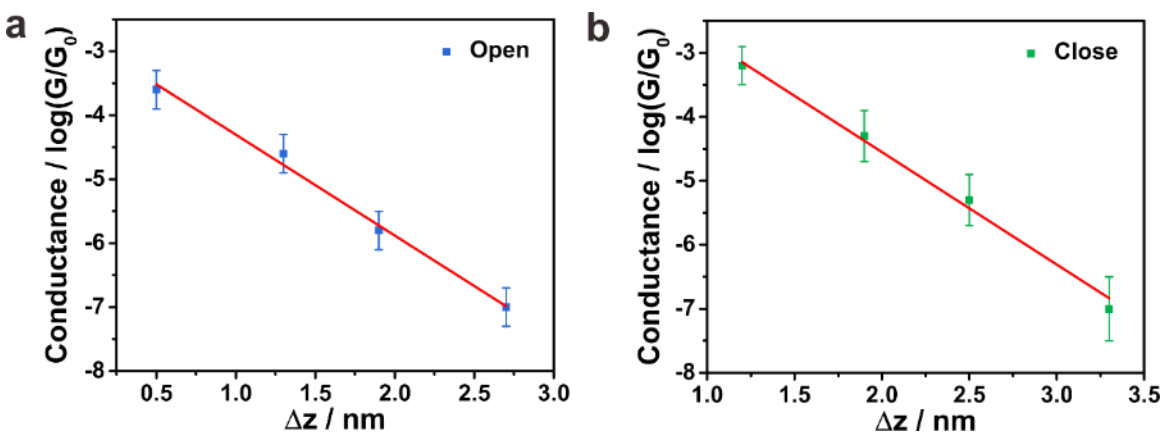


Figure S14. Tunneling decay constant fitting for the measured (a) opening and (b) closing processes of the **OAE** series.

Single molecule charge transport may originate from different mechanisms even in the same junction geometry. Therefore, we chose the **OAE** series extended only to **OAE5**, for which previous data established that the super-exchange mechanism still predominates.¹⁰ Using the measured conductance data, we are able to obtain the tunneling decay constant β of the opening and closing processes, as shown in Figures S14(a) and Figure S14(b), respectively. The fitted β values of the opening and closing processes are $3.6 \pm 0.2 \text{ nm}^{-1}$ and $4.0 \pm 0.2 \text{ nm}^{-1}$, respectively. Both values are close to those calculated by Zhao et al.,¹⁰ indicating that the super-exchange tunneling is indeed the major contribution from **OAE2** to **OAE5**. Moreover, we also adopted the β value of the hopping mechanism obtained previously from **OAE6** to **OAE9** by Zhao et al.,¹⁰ to extend to the short **OAE** series for calculating the hopping contribution. It was found that the hopping contributions from **OAE2** to **OAE4** are 0.093%, 0.851% and 12.3%, respectively, as shown in Figure S15. Therefore, the hopping contributions in **OAE2** and **OAE3** can be totally eliminated, while in **OAE4** and **OAE5** they cannot be neglected.

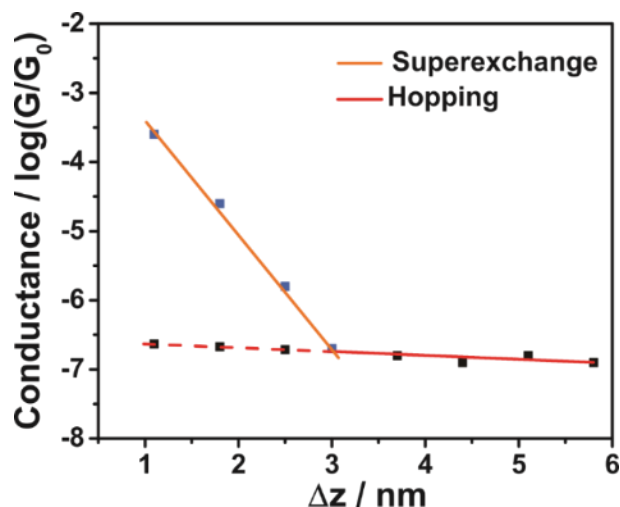


Figure S15. Hopping contribution fitted for shorter **OAE** series.

Nevertheless, although this work mainly focused on the through-space tunneling between the pair of electrodes and through-molecule tunneling, the ballistic and hopping tunneling both belong to the latter, which both originate from the molecular junction configuration.

9. Calculation of the through-molecule tunneling contributions of the OAE series.

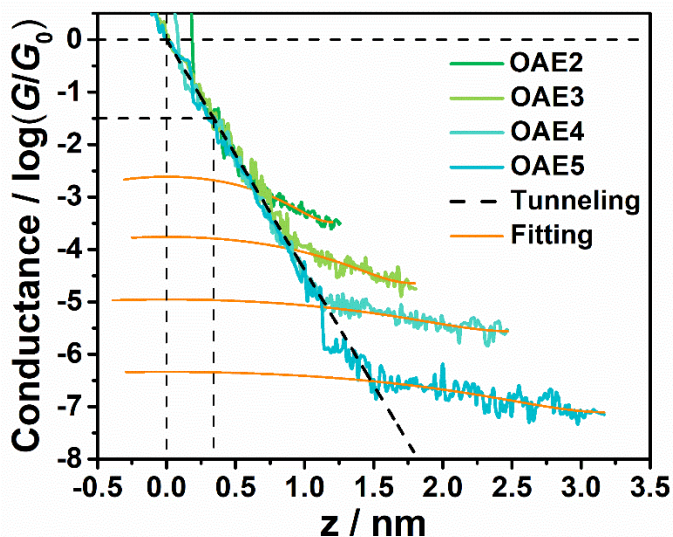


Figure S16. Calculation of through-molecular tunneling contribution of the **OAE** series.

We assumed that the molecular junction configurations in the lower panels of Figures S8(a) and S8(b) are typical configurations when the molecule has not been fully stretched in a relatively small gap between the pair of electrodes. Therefore, both the direct and molecular tunneling could contribute to the total conductance. Since we had calibrated the absolute distance scale, the

conductance evolution with an exact electrode gap size can be determined. Hence, here we discuss the shoulder feature around $10^{-1.5} G_0$ in Figure 2B in the main text, and the specific electrode gap size can be deduced by equation (5), which z will be 0.341 nm.

As shown in Figure S16, the through-molecule tunneling contribution can be calculated according to equations (8) to (11) for such a gap, and we found that the molecular tunneling contributions around $10^{-1.5} G_0$ of **OAE2** to **OAE5** are about $10^{-2.68} G_0$, $10^{-3.79} G_0$, $10^{-4.96} G_0$ and $10^{-6.34} G_0$, respectively, which suggests that the through-molecule tunneling contributes 6.61% for **OAE2**, 0.513% for **OAE3**, 0.0347% for **OAE4** and 0.00144% for **OAE5**. Therefore, the case of **OAE2** confirmed the former theoretical prediction, suggesting that through-space tunneling predominates, while molecular tunneling cannot be neglected. However, in longer **OAE** molecules the through-space tunneling around $10^{-1.5} G_0$ predominates, and their molecular tunneling can be neglected. That is probably the reason that there is no other shoulder feature around $10^{-1.5} G_0$ for all other longer **OAE** molecules. In conclusion, the through-space tunneling contributes mostly in the smaller gap beyond the molecular junction is fully stretched.

10. The transition in other conjugated systems.

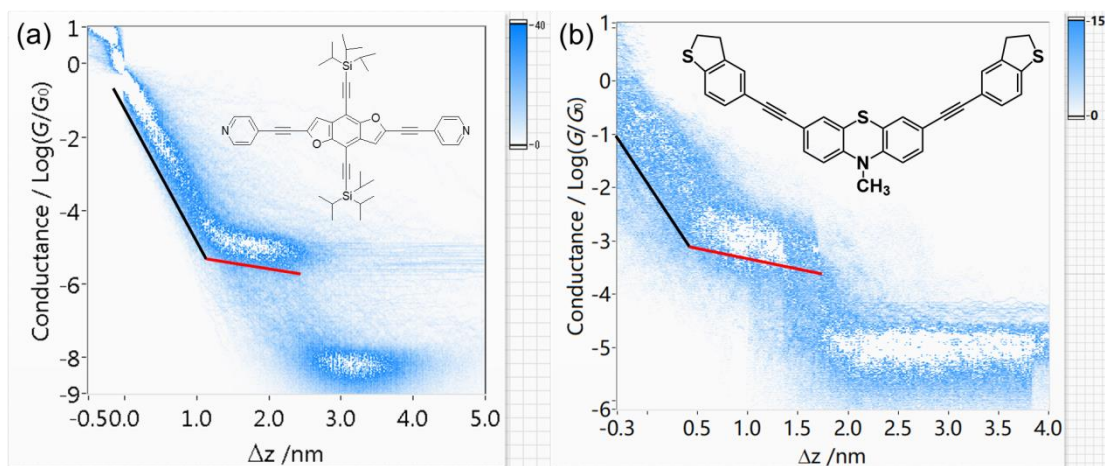


Figure S17. The conductance-distance histogram of the closing process of (a) the cruciform benzodifuran molecule and (b) phenothiazine derivative. Both of the histogram shows two distinct different regimes of firstly molecular tunneling (labelled by red line) then transiting to through-space tunneling (labelled by black line) during the electrodes approaching.

There are examples of other rigid conjugated molecules exhibiting the same closing behaviour as the **OAE** series. The cruciform benzodifuran molecule¹¹ and the phenothiazine derivatives¹² for which we have published their conductance features in the opening process, also showed prominent transition features in the closing process, as shown in Figure S17 (those data have not been published previously). The transition distance from Figure S17(a) of the cruciform benzodifuran molecule is about 1 nm; however, the molecular length is 2.2 nm. Figure S17(b) shows the transition distance of the phenothiazine derivative is about 0.5 nm; however, the molecular length is 2.1 nm. These data suggest that this physical phenomenon of transition is common in conjugated systems and highly depends on the chemical structure of the molecular junctions.

References

1. Hong, W., Manrique, D.Z., Moreno-García, P., Gulcur, M., Mishchenko, A., Lambert, C.J., Bryce, M.R., and Wandlowski, T. (2012). Single molecular conductance of tolans: Experimental and theoretical study on the junction evolution dependent on the anchoring group. *J. Am. Chem. Soc.* *134*, 2292-2304.
2. Hong, W., Valkenier, H., Mészáros, G., Manrique, D.Z., Mishchenko, A., Putz, A., García, P.M., Lambert, C.J., Hummelen, J.C., and Wandlowski, T. (2011). An MCBJ case study: The influence of π -conjugation on the single-molecule conductance at a solid/liquid interface. *Beilstein J. Nanotechnol.* *2*, 699-713.
3. Untiedt, C., Caturla, M.J., Calvo, M.R., Palacios, J.J., Segers, R.C., and van Ruitenbeek, J.M. (2007). Formation of a metallic contact: Jump to contact revisited. *Phys. Rev. Lett.* *98*, 206801.
4. Trouwborst, M.L., Martin, C.A., Smit, R.H.M., Guédon, C.M., Baart, T.A., van der Molen, S.J., and van Ruitenbeek, J.M. (2011). Transition voltage spectroscopy and the nature of vacuum tunneling. *Nano Lett.* *11*, 614-617.
5. Kornilovitch, P.E., and Bratkovsky, A.M. (2001). Orientational dependence of current through molecular films. *Phys. Rev. B* *64*, 195413.
6. Toyoda, K., Morimoto, K., and Morita, K. (2006). First-principles study on current through a single π conjugate molecule for analysis of carrier injection through an organic/metal interface. *Surf. Sci.* *600*, 5080-5083.
7. Diez-Perez, I., Hihath, J., Hines, T., Wang, Z.-S., Zhou, G., Mullen, K., and Tao, N. (2011). Controlling single-molecule conductance through lateral coupling of [pi] orbitals. *Nat. Nanotechnol.* *6*, 226-231.
8. Beebe, J.M., Kim, B., Gadzuk, J.W., Daniel Frisbie, C., and Kushmerick, J.G. (2006). Transition from direct tunneling to field emission in metal-molecule-metal junctions. *Phys. Rev. Lett.* *97*, 026801.
9. Lu, Q., Liu, K., Zhang, H., Du, Z., Wang, X., and Wang, F. (2009). From tunneling to hopping: A comprehensive investigation of charge transport mechanism in molecular junctions based on oligo(p-phenylene ethynylene)s. *ACS Nano* *3*, 3861-3868.
10. Zhao, X., Huang, C., Gulcur, M., Batsanov, A.S., Baghernejad, M., Hong, W., Bryce, M.R., and Wandlowski, T. (2013). Oligo(aryleneethynylene)s with terminal pyridyl groups: Synthesis and length dependence of the tunneling-to-hopping transition of single-molecule conductances. *Chem. Mater.* *25*, 4340-4347.
11. Huang, C., Chen, S., Baruël Ørnsø, K., Reber, D., Baghernejad, M., Fu, Y., Wandlowski, T., Decurtins, S., Hong, W., Thygesen, K.S., *et al.* (2015). Controlling electrical conductance through a π -conjugated cruciform molecule by selective anchoring to gold electrodes. *Angew. Chem. Int. Ed.* *54*, 14304-14307.
12. Liu, J., Zhao, X., Al-Galiby, Q., Huang, X., Zheng, J., Li, R., Huang, C., Yang, Y., Shi, J., Manrique, D.Z., *et al.* (2017). Radical enhanced charge transport in single-molecule phenothiazine electrical junctions. *Angew. Chem. Int. Ed.* *56*, 13061-13065.